Structures 50 (2023) 978–997

Contents lists available at ScienceDirect

Structures

journal homepage: www.elsevier.com/locate/structures

# Improving the shear behavior of RC dapped-end beams using precast strain-hardening cementitious composite (P-SHCC) plates

Ahmed T. Baraghith *, Abdel-Hakim A. Khalil, Emad E. Etman, Reda N. Behiry

*Structural Engineering Department, Faculty of Engineering, Tanta University, Tanta, Egypt*

ARTICLE INFO

*Keywords:*
Dapped-end beams (DEBs)
Strain-Hardening Cementitious Composites (SHCC)
precast SHCC (P-SHCC) plates
Shear strength
Ductility
Serviceability
Strengthening

ABSTRACT

Dapped-end beams (DEBs) are frequently used in precast concrete structures in order to facilitate the construction procedures. However, premature failure is most likely to happen at their re-entrant corner owing to the immense shearing stresses in this region. To mitigate such a problem, a new strengthening system making use of Strain-Hardening Cementitious Composites (SHCC) material was utilized in this paper. For this purpose, an experimental study on ten DEBs specimens, including one defected un-strengthened specimen (BC), was prepared and tested under a monotonic 4-point loading protocol to assess the efficiency of the adopted strengthening system. The traditional reinforcement at the re-entrant corner was substituted by precast SHCC (P-SHCC) plates to upgrade the shear strength and serviceability of the tested DEBs. The P-SHCC plates were pre-cured for about 4 weeks before being used to mitigate any volumetric change issues related to SHCC. A slight amount of reinforcement was provided inside the P-SHCC plates to enhance their cracking behavior and avoid strain localization. The studied parameters were the scheme of P-SHCC plates at the re-entrant corner (continuous or intermittent/discontinuous), the orientation of P-SHCC plates (vertical or 45°-inclined), as well as their position with regard to the beam's cross-section (external or internal). The thickness of each external P-SHCC plate was kept constant at 20 mm so as to be easily incorporated into the concrete cover, whereas the internal P-SHCC plates had varied thicknesses (40, 55, or 70 mm). The test results revealed that providing DEBs with P-SHCC plates could significantly improve both shear capacity and the developed ductility. The gain in the ultimate load reached up to 91 % relative to the un-strengthened specimen (BC). Furthermore, a great reduction in the developed major shear crack width for all strengthened DEBs was attained. At the service load level, all strengthened DEBs showed a decreased crack width, with an average value of about 77 % compared to the specimen BC. Finally, two equations considering the contribution of P-SHCC plates were proposed to predict both the shear strength and the average crack width of the strengthened DEBs. The proposed equations showed good agreement with the experimental results.

## 1. Introduction

Recently, more and more advances in the construction community have been accomplished. One of these developments is the widespread usage of precast concrete (PC) in structural applications [1]. Compared to cast-in-situ concrete, PC has superior merits such as rapid construction, which is an imperative aspect, especially in adverse weather conditions, noise reduction, and its admirable appearance [2]. Usually, these structures are naturally not monolithic and imply a loss of structural continuity as they are composed of individual members assembled together by means of various connections. Dapped ends are broadly used in precast buildings, particularly in parking structures or bridges as one of these connections [3,4].

Beams rested on corbels, inverted *T*-beams, L-edge beams, or directly on columns with notched ends are so-called dapped-end beams (DEBs), as they are distinguished by an abrupt drop of the cross-section at their ends. The notch itself is known as the "dap" and the part of the beam that is above the dap is called the "nib" as depicted in Fig. 1. Dapped-end beams (DEBs), also known as recessed beams or half joints, have numerous benefits. As compared with an isolated beam supported at its bottom face, ease in the erection of PC structures is achieved when DEBs are used [5,6]. Moreover, a worthy lateral stability as well as a reduction in the overall construction height due to recessing at the ends are two other features that make DEBs more favorable in the manufacturing of PC structures [7–9].

* Corresponding author at: Structural Engineering Department, Faculty of Engineering, Tanta University, Tanta 31511, Egypt.
*E-mail addresses:* ahmed.baraghit@f-eng.tanta.edu.eg, ahmed_baraghit@yahoo.com (A.T. Baraghith).

https://doi.org/10.1016/j.istruc.2023.02.059
Received 12 December 2022; Received in revised form 5 February 2023; Accepted 11 February 2023
Available online 24 February 2023
2352-0124/© 2023 Institution of Structural Engineers. Published by Elsevier Ltd. All rights reserved.

**Nomenclature**

| | |
|---|---|
| $f_c^{'}$ | Concrete compressive strength for standard cylinder (MPa). |
| $d_{by}$ | The diameter of shear reinforcement (mm). |
| $k_w$ | The coefficient that considers the effect of shear reinforcement ratio. |
| $k_{f_c}$ | The coefficient that considers the effect of compressive strength of concrete. |
| $k_1$ | The bond coefficient, for smooth bars and 2.0 for deformed bar. |
| $k_2$ | The stress distribution coefficient, 1.2 for vertical web reinforcement and 1.0 for inclined web reinforcement. |
| $\rho_w$ | The web reinforcement ratio. |
| $\varepsilon_w$ | The tensile strain of shear reinforcement. |
| $S_l$ | The normalized slip strains. |
| $l_{av}$ | The average crack spacing (mm). |
| $c_s$ | The side concrete cover to the shear reinforcement (mm). |
| $b_w$ | The width of cross-section (mm). |
| $A_w$ | The area of web reinforcement ($mm^2$). |
| $s_y$ | The shear reinforcement spacing (mm). |
| s | The distance between stirrup legs (mm). |
| $S_{m\theta}$ | The average shear crack spacing (mm). |
| $C_x$ | The distance from the horizontal center line of the concrete cross-section to longitudinal reinforcements (mm). |
| $C_y$ | The distance from the center line of the concrete cross section to the inner edge of vertical reinforcement (mm). |
| $S_{mx}$ | The horizontal average shear crack spacing (mm). |
| $S_{my}$ | The vertical average shear crack spacing (mm). |
| $S_x$ | The spacing between longitudinal reinforcement (mm). |
| $S_y$ | The spacing between web reinforcement (mm). |
| $d_{bx}$ | The diameter of longitudinal bars (mm). |
| $\rho_y$ | The ratio of vertical reinforcement. |
| $\rho_x$ | The ratio of longitudinal reinforcement. |
| $\theta$ | The inclination angle of the diagonal shear crack. |

Nevertheless, owing to the sudden variation in geometry of the cross-section of these beams at their ends, an intense internal stress is generated particularly close to the weakened part (i.e., the re-entrant corner) of DEBs; specifically, when the nib section depth is below 0.45 times the un-dapped section depth [5,10–12]. The portions that are prone to severe stress concentration are named disturbed/discontinuity regions (D-regions) [13,14]. It is perfectly acceptable to the previous researchers that D-regions are completely different in behavior from B-regions. A linear strain distribution is achievable in B-regions, allowing the classic beam hypothesis to be applied, whereas in D-regions it cannot be due to the explicit nonlinearity of the strain distribution. D-region dies out at a distance that is approximately equal to the total depth of the dapped-end beam (H) beyond the nib (refer to Fig. 1). In such regions, the assumption that a plane section remains plane after bending is no longer valid, and consequently, St. Venant's principle could be satisfactory applied [4,15,16].

In accordance with the Pre-stressed Concrete Institute (PCI) Design Handbook [17], Fig. 2 schematically represents the common five potential modes of failure considered in DEBs. These separately investigated failure modes are: (1) Flexure (cantilever bending) and axial tension failure in the nib; (2) Vertical direct shear failure at the junction between the nib and un-dapped portion of the beam; (3) Diagonal tension failure propagated from the re-entrant corner; (4) Diagonal tension failure in the nib; and (5) Diagonal tension failure starting from the bottom corner of the beam's un-dapped zone [2,3,7,12,18]. Regarding the aforementioned modes of failure, D-regions in DEBs are exposed to shear failure with no warnings prior to B-regions due to the reduction of effective area at the nib. So, appropriate reinforcements and necessary precautions should be well-considered (refer to Fig. 3); otherwise, poor serviceability will be obtained and a sudden collapse will occur [19]. Due to their importance in precast concrete constructions, DEBs were of interest to several researchers in recent decades to upgrade their efficiency. The urgent need to promote the capacity of DEBs may be attributed to some major durability issues and even collapses that have been recorded in DEB structures [20,21], despite pursued standard concrete details and extensive previous experimental research [8–10,18,22–32].

Using different techniques, numerous studies were performed focused on enhancing the shear performance of reinforced concrete dapped-end beams. These techniques include externally bonded steel plates [3], Fiber Reinforced Polymers (FRPs) [2,3,14,33,34], and external prestressing [12]. Lately, an experimental program consisting of eight specimens was performed by Atta and Taman [12] to evaluate the effectiveness of the external prestressing technique with different configurations (horizontal, vertical, or inclined) in retrofitting DEBs. Based on their experiments, they concluded that the external prestressing technique is capable of enhancing both the strength and ductility of such beams. Instead, FRPs are considered another option to increase the ultimate capacity of DEBs due to their superior features such as: high strength-to-weight ratio, ease of installation, and advanced corrosive resistance [19]. Fifty rectangular DEBs were tested by Taher [3] with different retrofitting techniques, such as externally bonded steel plates and FRPs. In his research, it was stated that FRPs were the most practical solution for improving the capacity of DEBs. Furthermore, Nagy-Gyorgy et al. [2] and Tan [33] confirmed experimentally that FRP with various configurations had the ability to satisfactory




**Fig. 1.** Typical geometry and aspects related to dapped-end beams.

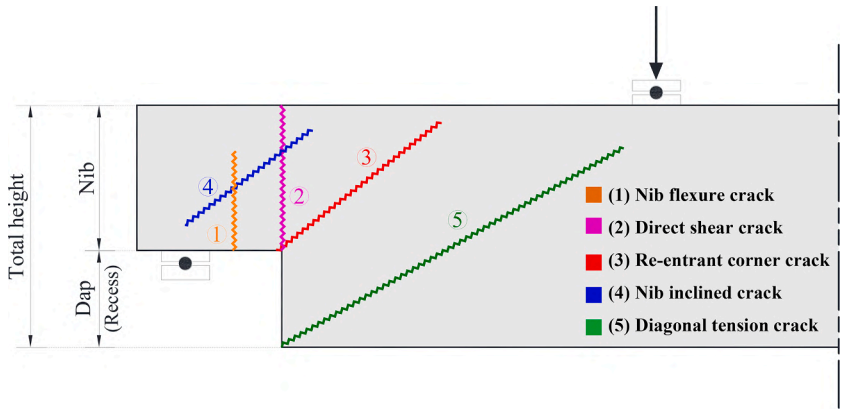
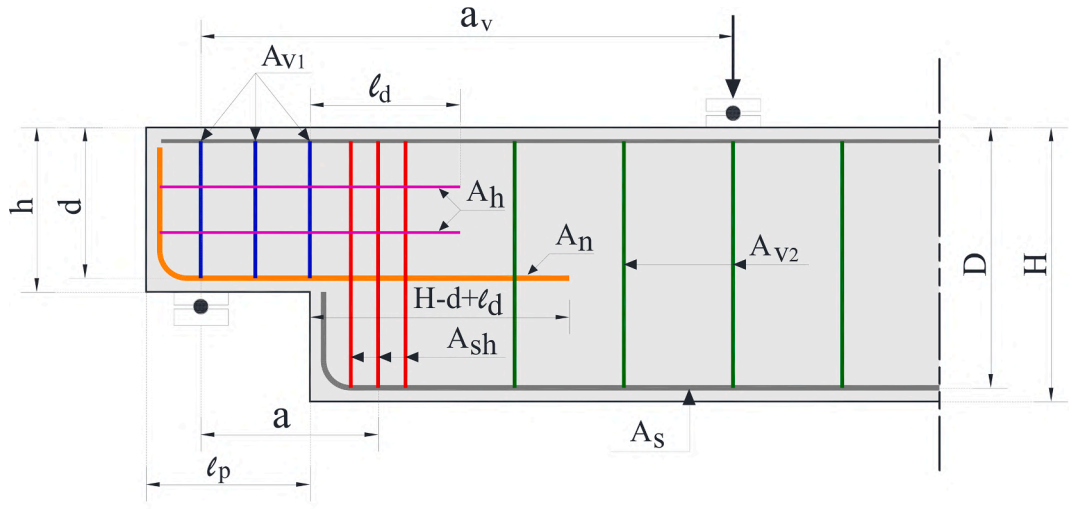
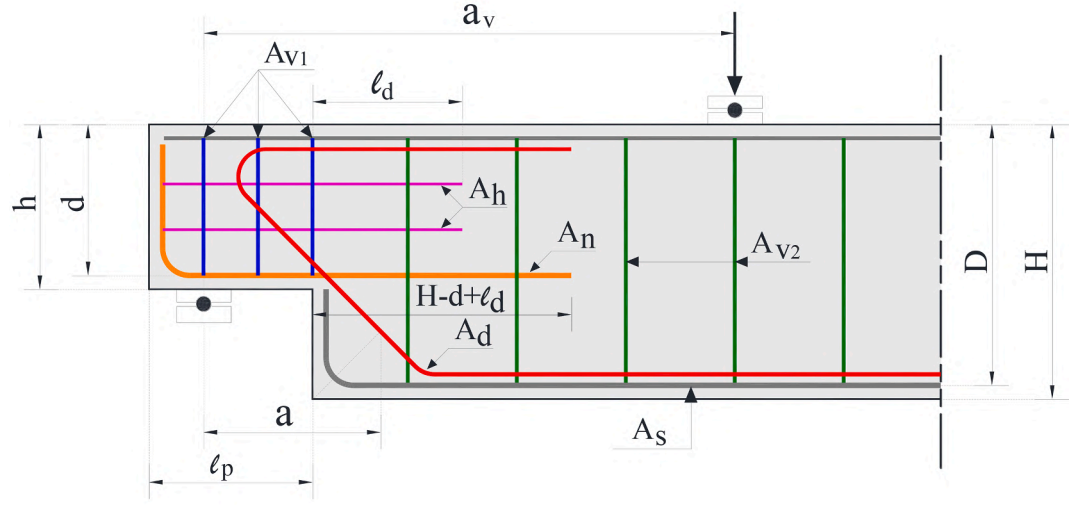



**Fig. 2.** Potential modes of failure in dapped-end beams according to PCI Design Handbook [17].




a. Reinforcement layout of DEBs using hanger bars at the re-entrant corner.




b. Reinforcement layout of DEBs using diagonal bars at the re-entrant corner.

**Fig. 3.** Different reinforcement layouts for DEBs according to PCI Design Handbook [17].

improve the shear capacity of deficient DEBs.

Nonetheless, it should be considered that all the aforementioned strengthening techniques had a series of pros and cons. Externally bonded steel plates, in addition to external prestressing techniques require higher skill in the application process. Moreover, they are easily susceptible to corrosion, resulting in hastening the damage to the

structure [35]. As for FRPs, although their advanced characteristics, they are costly and have a low temperature resistance. Too, premature failure of FRP strengthening system is more probably to happen as a result of debonding at their ends [36,37].

Nowadays, a novel category of fiber reinforced cementitious composites called Engineered Cementitious Composites (ECC) has received more attention to overcome the above-mentioned shortcomings related to the available strengthening materials. In 1992, ECC were firstly introduced by Li and co-workers depend on micromechanics theory [38,39]. Strain-hardening Cementitious Composite (SHCC) is an alternative designation for ECC, given by the RILEM TC HFC Technical Committee in 2006, highlighting its tensile pseudo strain-hardening behavior instead of softening, reaching about 3–5 % ultimate strain capacity under uniaxial tensile tests [40–43]. Typically, SHCC mix contains a binder (e.g., cement and silica fume (SF)), sand, superplasticizer (SP), and non-metallic fibers with a volume fraction less than 2 % [44]. SHCC is an exciting class of materials has significantly higher damage tolerance capacity, ductility, durability, and energy absorption capacity due to their multiple fine microcracking behavior [45,46]. This explains the ongoing rapid spread of SHCC as a retrofitting or new construction material in the structural applications (beams, columns, slabs, etc.) [47–62]. As yet, the applications of SHCC are still evolving.

To the authors' knowledge, very limited experimental investigations on SHCC-strengthened dapped-end beams have been reported [63,64]; despite the superior features of SHCC materials. Accordingly, the current research aims to study the improvements in the shear strength as well as the serviceability of DEBs provided with either external or internal precast SHCC (P-SHCC) plates near the re-entrant corner (i.e., the weakest portion in DEBs). Consequently, ten specimens were cast and tested under a 4-point loading protocol. The main studied parameters in the present study were the scheme, orientation, position, and thickness of P-SHCC plates. The structural assessment of the strengthened DEBs considered the ultimate load capacity, crack width, and ductility. Finally, two proposed equations for predicting the ultimate shear capacity and the average shear crack width of the strengthened DEBs were made.

## 2. Experimental work program

### 2.1. Test dapped-end beams

To get a clear and accurate assessment on the feasibility of the precast SHCC (P-SHCC) plates as a strengthening system for dapped-end beams (DEBs), an experimental program involving ten specimens was performed. Fig. 4 shows the typical concrete dimensions in addition to the reinforcement detailing for all un-strengthened and strengthened DEBs, in which all tested beams had the same concrete dimensions. The wholly span of all beams was 2400 mm incorporating 300 mm dapped and 2100 mm un-dapped lengths while the center-to-center span was 2200 mm. To simulate reality in actual bridge applications, the location of the center of the supporting point does not typically accord with the nib mid-point but is instead slightly shifted towards the outer edge. The cross-sectional dimensions of the dapped/nib portion were 150 mm width by 200 mm total depth, while the un-dapped portion was 150 mm width by 400 mm total depth. It is worth mentioning that the ratio between the nib depth and the overall depth was 0.50, which is in line with the minimum value specified by Wang et al. [10].

A total of 2 bars of 18 mm diameter were included as longitudinal flexural reinforcement, while 2 bars with a diameter of 12 mm were provided as longitudinal compression reinforcement. These flexural reinforcements were chosen in such a way to avoid flexural failure of the full depth section of DEBs. The tension reinforcements were 90-degree hooked up to prevent bar slippage, whereas the compression reinforcements were 90-degree hooked down into the dapped-end in order to exclude the flexural failure in the nib. U-bar side reinforcements (10 mm in diameter) with sufficient development lengths were supplied to avoid the direct vertical shear failure at the intersection between the dapped and un-dapped zones. Diagonal tension failure in the nib of the tested DEBs was banned by using vertical stirrups made of smooth bars having 8 mm diameter and spaced at 80 mm. While stirrups of 8 mm diameter spaced every 200 mm were used to overcome diagonal tension failure originating from the bottom corner of the un-dapped region. The right shear span was reinforced with vertical stirrups of 8 mm diameter smooth bars and spaced every 100 mm to eliminate any shear failure at the right shear span zone even after strengthening the dapped zone (refer to Fig. 4). It is worth stating that all the required development lengths were calculated based on the provisions stipulated as per *ACI* 318–19 code [65], as given by Eq. (1).

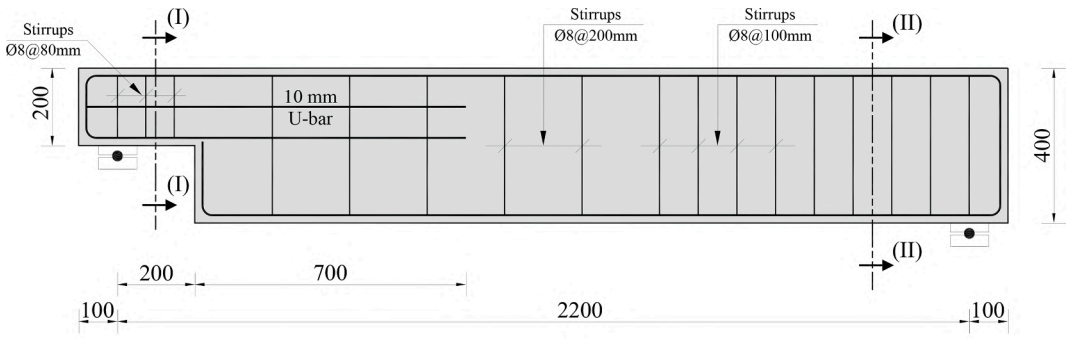
$$L_d = \frac{f_y \psi_t \psi_e \psi_g}{2.10\lambda\sqrt{f'_c}}\varphi \tag{1}$$

where $L_d$ is the development length of a bar with diameter $\varphi$(mm); $\psi_t$ is the reinforcement location factor to account for the effect of the casting position (1.30 if more than 300 mm of fresh concrete is placed below horizontal reinforcement, 1.00 for others); $\psi_e$ is a coating factor reflecting the effects of a bar coating type (1.20 for epoxy-coated reinforcement, 1.00 uncoated or galvanized reinforcement); $\psi_g$ is the reinforcement grade factor accounting for the yield strength of the reinforcement (1.00 for grade 280 or grade 400, 1.15 for grade 550, 1.30 for grade 690); $\lambda$ is modification factor represents the concrete type (1.00 for normal weight concrete, 0.75 for lightweight concrete); $f'_c$ specified cylinder compressive strength of concrete (MPa); $f_y$ is specified yield strength for reinforcement (MPa).

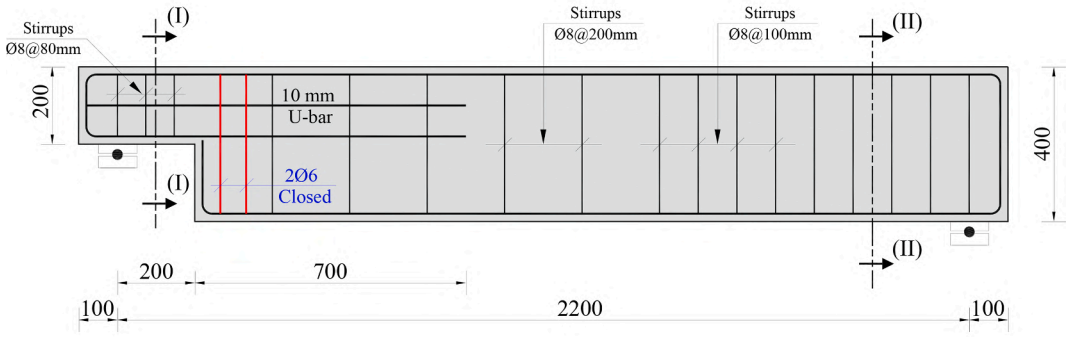
As shown in Table 1, the experimental work program was divided into four groups. The un-strengthened reference group No. 1 consisted of three specimens: one defected and two properly detailed DEBs. The defected specimen (BC) was left vacant of shear reinforcements at the re-entrant corner. While the remaining two DEBs (BC-H and BC-D) were correctly designed, confirming PCI guidelines [17], with traditional reinforcements (hanger or diagonal) to resist the diagonal crack emanating from the re-entrant corner. The first hanger reinforcement was kept as close as possible to the nib's edge, which is in accordance with Wang et al. recommendations [10]. Group No. 2 contained two defected specimens strengthened by external P-SHCC plates (40 mm thickness) with different schemes (continuous or intermittent/discontinuous). Furthermore, one additional group (group No. 3), the same aspects as group No. 2, involved two defected DEBs but was strengthened by 45°-inclined P-SHCC plates. Lastly, group No. 4 contains three defected DEBs strengthened by an internal P-SHCC plate with different thicknesses (40, 55, or 70 mm).

### 2.2. Material properties

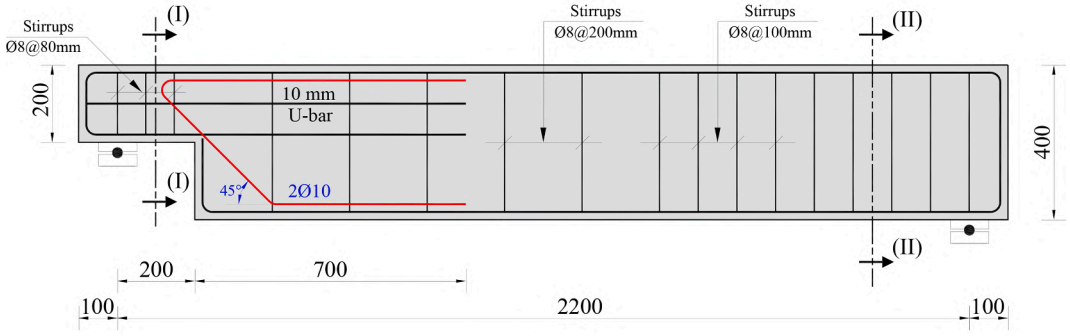
To achieve the same concrete properties, all tested dapped-end beams (DEBs) were cast with each other using ready-mix concrete of target cylinder strength of 30 MPa. Then, all DEBs were wet cured under the same circumstances for two weeks, then left exposed to air drying until the testing day. According to the data sheet provided by the supplier, the mix proportions are listed in Table 2, where Portland cement (Type I) was used as a binder. The concrete mix contained natural sand and crushed pink limestone type 1 (maximum aggregate size 10 mm) as fine and coarse aggregates, respectively. As well, the used water/binder ratio (w/b) was about 0.50. All DEBs were tested in three consecutive days to avoid any slight differences in concrete compressive strength. Nine concrete cylinders of 150 mm diameter and 300 mm height were prepared during the casting of all specimens and subjected to the same curing conditions in order to estimate the mechanical properties of the used concrete. At the testing day, uniaxial compression tests were carried out in accordance with ASTM C39/C39M-21 [66] and the average compressive strength for cylinders was 32.60 MPa. To determine the tensile strength of the used concrete, two tests were used: the flexural



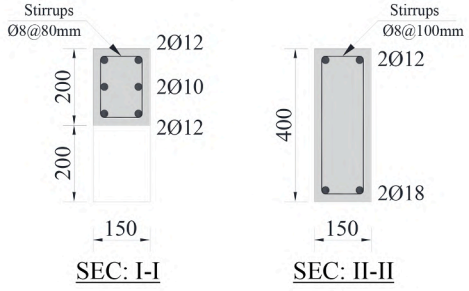

a. All specimens expect for BC-H and BC-D.




b. Specimen BC-H.




c. Specimen BC-D.




d. Cross-sections.

**Fig. 4.** Geometry and steel reinforcements of the tested specimens (All dimensions in mm).

**Table 1**
Test matrix.

| Group No. | Specimen codification | Characteristics | Objectives |
|---|---|---|---|
| G1 | BC | Defected dapped-end beam (DEB) vacant of shear reinforcements at the re-entrant corner. | Reference un-strengthened group. |
| | BC-H | Properly detailed DEB provided with hanger reinforcements at the re-entrant corner confirming PCI guidelines [17]. | |
| | BC-D | Properly detailed DEB provided with diagonal reinforcements ($\alpha = 45°$) at the re-entrant corner confirming PCI guidelines [17]. | |
| G2 | BUE-H1-40 | DEB strengthened by external vertical P-SHCC plates (20 mm thickness/ each side) with continuous scheme. | Studying the effect of using precast strain-hardening cementitious composite (P-SHCC) plates with different schemes. |
| | BUE-H2-40 | DEB strengthened by external vertical P-SHCC plates (20 mm thickness/ each side) with intermittent/ discontinuous scheme. | |
| G3 | BUE-D1-40 | DEB strengthened by external diagonal P-SHCC plates (20 mm thickness/ each side) with continuous scheme. | Studying the effect of P-SHCC plates orientation. |
| | BUE-D2-40 | DEB strengthened by external diagonal P-SHCC plates (20 mm thickness/ each side) with intermittent/ discontinuous scheme. | |
| G4 | BUI-D1-40 | DEB strengthened by internal diagonal P-SHCC plate (40 mm thickness centered to the beam's cross-section) with continuous scheme. | Studying the effect of P-SHCC plate position with different thicknesses. |
| | BUI-D1-55 | DEB strengthened by internal diagonal P-SHCC plate (55 mm thickness centered to the beam's cross-section) with continuous scheme. | |
| | BUI-D1-70 | DEB strengthened by internal diagonal P-SHCC plate (70 mm thickness centered to the beam's cross-section) with continuous scheme. | |

test according to ASTM C293/C293M-16 [67] and the cylinder splitting tensile test as per ASTM C496/C496M-17 [68]. The average modulus of rupture strength and split cylinder strength were 6.96 and 4.97 MPa, respectively. The average modulus of elasticity and Poisson's ratio as per ASTM C469/C469M-14 [69] were 26.08 GPa and 0.195. Table 3 summarizes the mechanical properties of the hardened normal strength concrete (NSC) and SHCC materials.

In this paper, Precast Strain-hardening Cementitious Composites (P-SHCCP) plates were used as a strengthening system for the tested dapped-end beams. They were composed of SHCC material as well a small amount of reinforcement (4 mm in diameter). The design mix of the used SHCC materials was developed through previous work by Baraghith et al. [51] and presented in Table 2. A cubic meter of SHCC material contains a binder of 1090 kg Ordinary Portland cement 52.5R and 109 kg silica fume. A weight of 654 kg/m$^3$ continuously graded fine sand with a diameter less than 0.5 mm was used as fine aggregates, whereas coarse aggregates were deliberately eliminated as they increase crack width, which is contradictory to the property of SHCC and can affect the fiber dispersion. A volume fraction of 1.5 % Polypropylene micro-fibers (PP) with 0.01 mm diameter and 12 mm length was added. According to the manufacturer's data sheets, the mechanical characteristics of the used PP fibers are 150 MPa for tensile strength, 3.0 GPa for elastic modulus, and 8 % for elongation. Water/binder ratio (w/b) was about 0.27, and a superplasticizer based on polycarboxylic ether was used as a high water-reducing admixture to improve the matrix flowability. The mechanical properties of the used SHCC, such as the average compressive strength for cylinders, modulus of elasticity, and Poisson's ratio, were determined based on the aforementioned standards [66,69] used in traditional concretes, on which their values were 61.45 MPa, 19.04 GPa, and 0.252, respectively. As the tensile strength is the prime merit of the used SHCC material, three different tests were performed to identify their value. These tests were a flexural test in accordance with ASTM C293/C293M-16 [67], a cylinder splitting tensile test as per ASTM C496/C496M-17 [68], and a uniaxial tensile test according to ASTM D2936-20 [70]. The average modulus of rupture, split cylinder, and direct tensile strength were 13.53, 9.42, and 8.32 MPa, respectively (refer to Table 3). The specimen dimensions, test setup, and the obtained stress–strain curves of the SHCC material under uniaxial tensile testing are depicted in Fig. 5.

Ribbed reinforcing bars of 12 mm and 18 mm diameters were used to construct the reinforcement cages, whereas normal mild bars with diameters of 8 mm and 10 mm were used as a web reinforcement. In addition, 4 mm-diameter plain smooth bars were the reinforcements embedded inside the P-SHCC plates. The mechanical properties of the used reinforcement bars (yield strength, ultimate strength, and modulus of elasticity) were experimentally measured by testing three typical specimens for each diameter using a universal testing machine with a capacity of 200 kN and a loading rate of 0.1 mm/s with accordance to ASTM A615/ A615M-16 [71], then summarized in Table 4. It is worth mentioning that the yield strength of the deformed bars was determined based on the 0.2 % offset method.

### 2.3. Fabrication of strengthened dapped-end beams

Fig. 6 illustrates the different schemes as well as the dimensions of the Precast Strain-hardening Cementitious Composites (P-SHCC) plates used in order to strengthen the tested dapped-end beams (DEBs). These P-SHCC plates were made up of prismatic SHCC plates with a rectangular cross-section that were lightly steel-reinforced with 4 mm plain smooth bars. Regardless of the P-SHCC plate thickness, the reinforcement ratio was kept constant and equaled 0.84 % relative to the cross-sectional area of the P-SHCC plate. The strengthening plates were

**Table 2**
Mix proportions of NSC and SHCC materials (kg/m$^3$).

| Concrete mix | W/B | Cement | Sand | Coarse pink limestone | Water | Silica fume | Super-plasticizer | PP Fiber (12 mm) |
|---|---|---|---|---|---|---|---|---|
| **NSC** | 0.50 | 400 | 654 | 980 | 200 | — | — | — |
| **SHCC** | 0.27 | 1090 | 654 | — | 327 | 109 | 24 | 12 |

NSC = Normal Strength Concrete; SHCC = Strain-Hardening Cementitious Composites; W/B = water/binder ratio; B = cement + silica fume.

**Table 3**
Mechanical properties of the hardened NSC and SHCC materials.

| Mechanical properties and test method | Samples' description | NSC Sample (1) | Sample (2) | Sample (3) | Average value | SHCC Sample (1) | Sample (2) | Sample (3) | Average value |
|---|---|---|---|---|---|---|---|---|---|
| Compressive strength ($f_c'$), MPa ASTM C39/C39M-21 [66] | Cylinder of 150 mm diameter and 300 mm height | 32.07 | 31.98 | 33.75 | 32.60 | 61.32 | 61.21 | 61.82 | 61.45 |
| Flexural strength ($f_f$), MPa ASTM C293/C293M-16 [67] | Prism of 600 × 100 × 100 mm | 7.02 | 6.46 | 7.40 | 6.96 | 13.92 | 13.10 | 13.58 | 13.53 |
| Splitting tensile strength ($f_{st}$), MPa ASTM C496/C496M-17 [68] | Cylinder of 150 mm diameter and 300 mm height | 4.79 | 4.83 | 5.29 | 4.97 | 9.36 | 9.38 | 9.52 | 9.42 |
| Modulus of elasticity ($E$), GPa ASTM C469/C469M-14 [69] | Cylinder of 150 mm diameter and 300 mm height | 25.93 | 26.13 | 26.18 | 26.08 | 19.06 | 18.95 | 19.11 | 19.04 |
| Poisson ratio ($\upsilon$) ASTM C469/C469M-14 [69] | Cylinder of 150 mm diameter and 300 mm height | 0.193 | 0.192 | 0.200 | 0.195 | 0.250 | 0.252 | 0.254 | 0.252 |
| Uniaxial tensile strength ($f_{ti}$), MPa ASTM D2936-20 [70] | Dog-bone of 330 × 30 × 30 mm | NA | NA | NA | NA | 8.11 | 8.24 | 8.61 | 8.32 |
| Ultimate tensile strain ($\varepsilon_{ti}$), ($\mu\varepsilon$) ASTM D2936-20 [70] | Dog-bone of 330 × 30 × 30 mm | NA | NA | NA | NA | 1882 | 1886 | 1893 | 1887 |

NSC = Normal Strength Concrete; SHCC = Strain-Hardening Cementitious Composites, NA = Not Applicable.

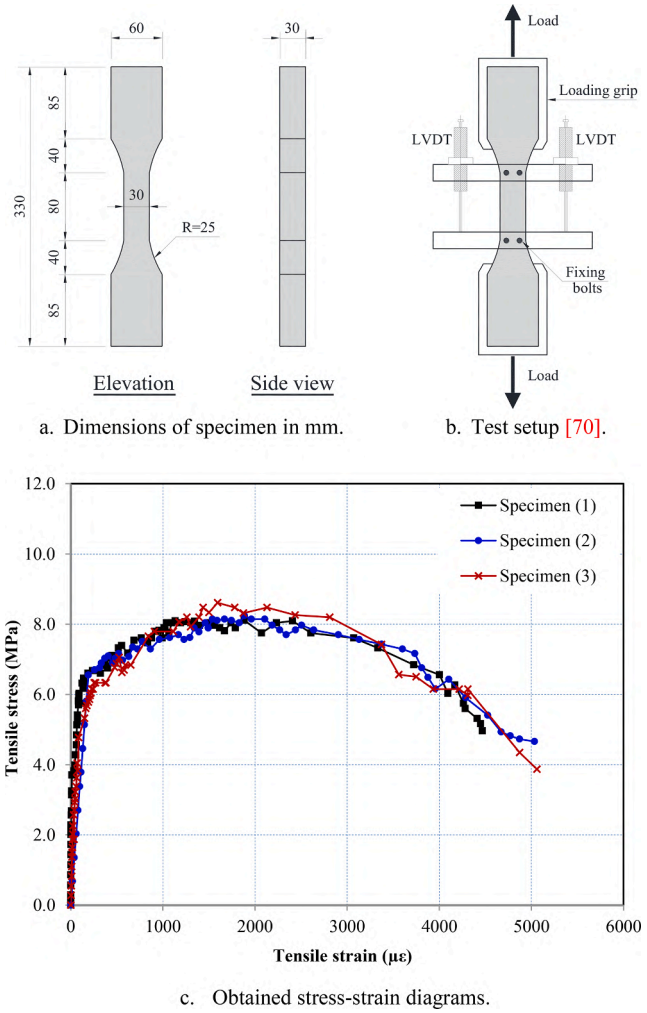


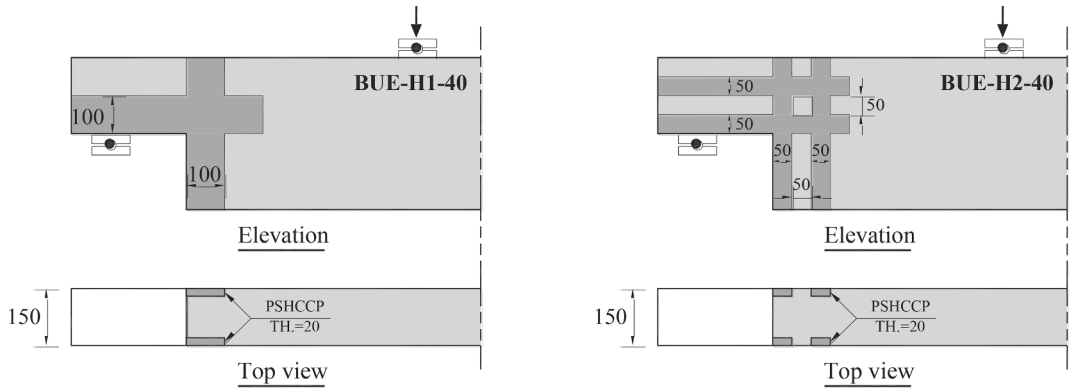

**Fig. 5.** Uniaxial tensile testing of the dog-bone shaped SHCC specimens.

**Table 4**
Properties of the steel material determined in laboratory tests.

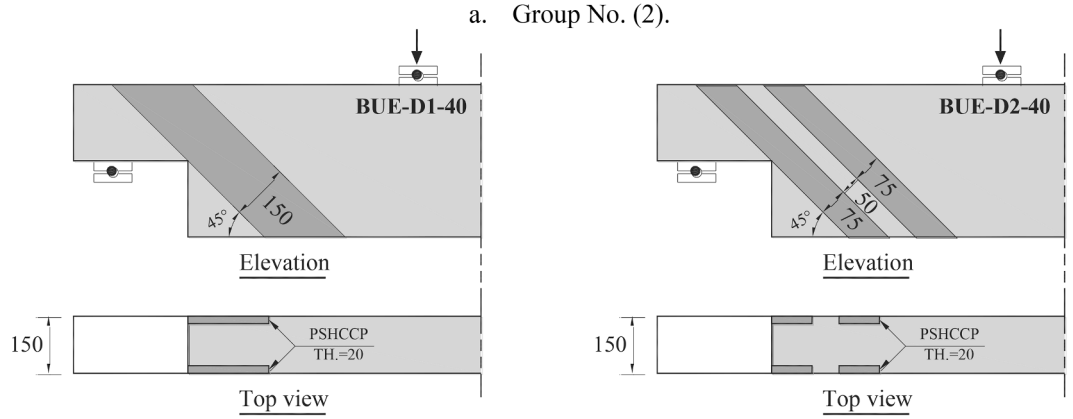
| DiameterΦ (mm) | Yielded strength $f_y$(MPa) | Ultimate strength $f_u$(MPa) | Yielded strain $\varepsilon_y$(με) | Young's modulus $E_s$(GPa) |
|---|---|---|---|---|
| 4 | 280 | 405 | 1400 | 200 |
| 6 | 280 | 395 | 1400 | 200 |
| 8 | 283 | 383 | 1408 | 201 |
| 10 | 280 | 359 | 1400 | 200 |
| 12 | 440 | 623 | 2178 | 202 |
| 18 | 420 | 605 | 2069 | 203 |

positioned at the outermost of the cross-section of specimens in groups No. 2 and No. 3; whereas kept centered to the cross-section of specimens in group No. 4. Indeed, for comparison purposes, the width of the P-SHCC plates in all strengthened DEBs, which is perpendicular to the expected crack line, was almost kept constant at 150 mm.

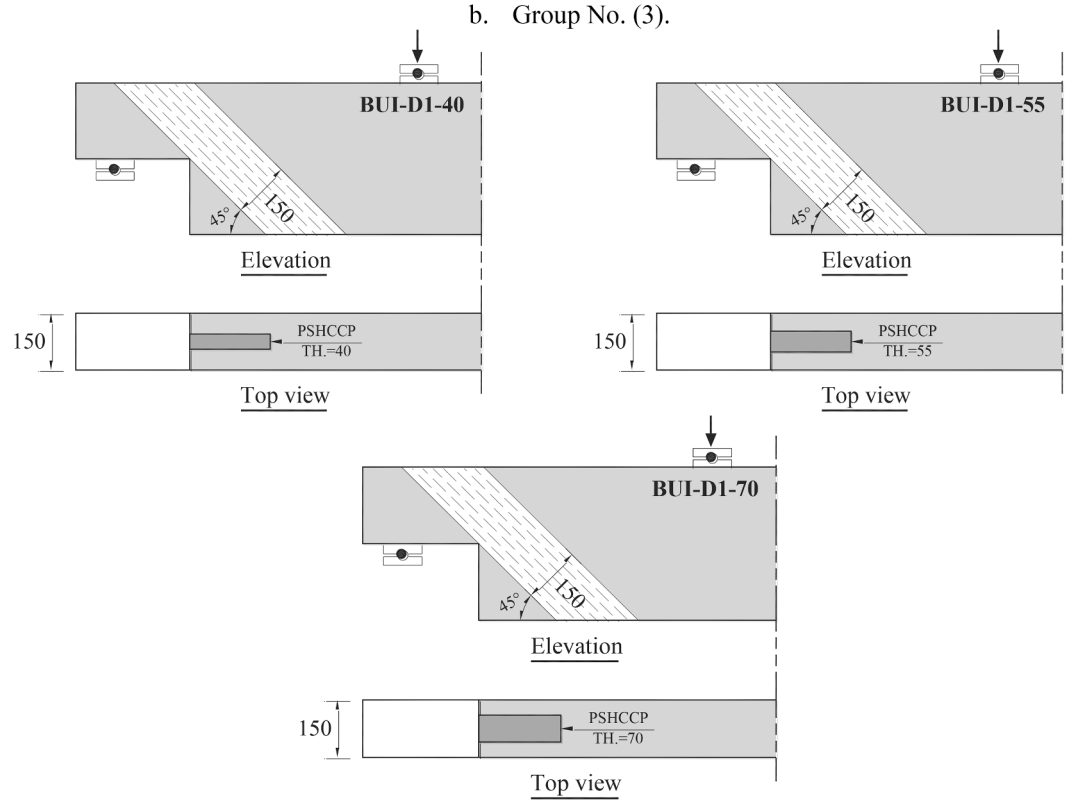
The step-by-step fabrication process of all DEBs strengthened with P-SHCC plates is depicted in Fig. 7. First, according to the pre-assigned dimensions of the P-SHCC plates, the horizontal wooden formworks shown in Fig. 7(a) were prepared. Second, the SHCC material proportions were mixed in a Hobart horizontal mixer with a 20-liter capacity and then poured to the middle of the desired thickness in the pre-prepared mold, hence the internal reinforcements were positioned. Following that, the remaining SHCC material was poured on one side of the formwork and then allowed to flow to the other side on its own to obtain the final P-SHCC plate thickness as shown in Fig. 7(b). It should be emphasized that all P-SHCC plates were cast using the same above-mentioned casting procedures to eliminate any dissimilar fiber distribution. Third, the P-SHCC plates were demolded after 24 h, then wet cured by immersing in water for about 4 weeks according to JSCE recommendations [72], and thereafter allowed to air dry to avoid the early-age high shrinkage phenomenon of the SHCC material (refer to Fig. 7 (c)). After the curing process, the P-SHCC plate surfaces planned to be adjacent to the substrate concrete were roughened to an average amplitude of about 5 mm by chisel and then cleaned using compressed air. Finally, the P-SHCC plates and the reinforcing cage were assembled




a. Group No. (2).



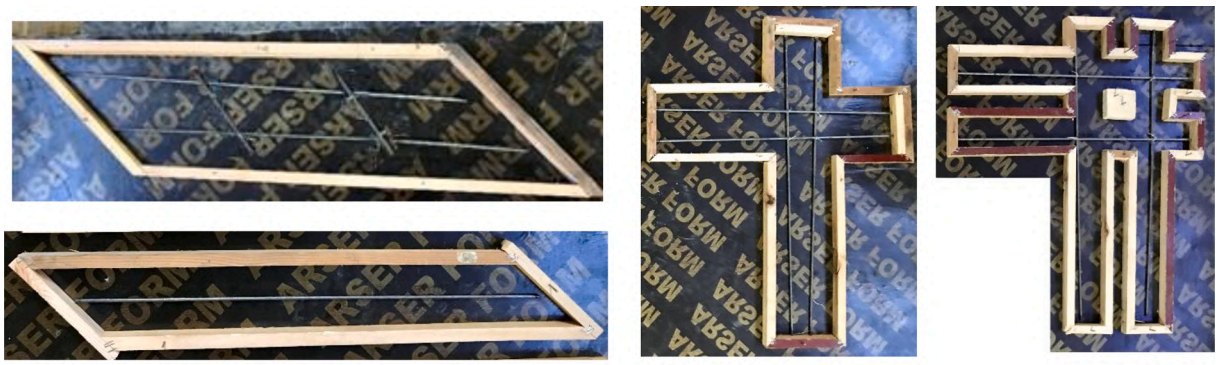

b. Group No. (3).



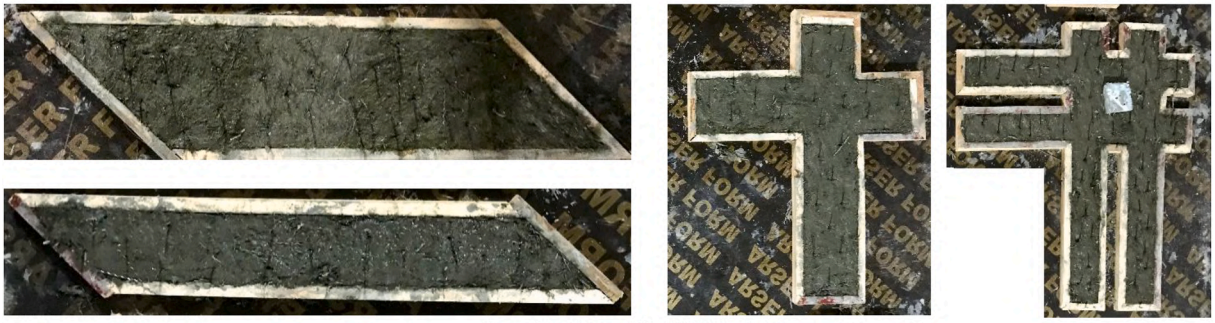

c. Group No. (4).

**Fig. 6.** Schemes and dimensions of the P-SHCC plates used in strengthening DEBs (All dimensions in mm).

together and positioned in wooden forms to be ready for concrete core casting, as depicted in Fig. 7(d). Just before concrete casting, all P-SHCC plate was coated with an epoxy resin (MasterBrace ADH 1414 [73]) to increase the bond strength with the substrate concrete. It is worth mentioning that all specimens were cured for two weeks, then subjected to air-drying until the testing day. Moreover, all tests were carried out over three continuous days in order to limit any variations in the ultimate strengths for concrete and SHCC material.



a. Formwork and reinforcements of P-SHCC plates.



b. Casting of P-SHCC plates.



c. P-SHCC plates after curing.



d. Example of fixing the internal P-SHCC plate with the reinforcement cage.

**Fig. 7.** Strengthening application process.

### *2.4. Test setup and instrumentation*

One bay of a three-dimensional steel frame was equipped and hence used to perform the testing. All dapped-end beams (DEBs) were incrementally loaded under a monotonic 4-point loading protocol, as shown in Fig. 8. Just prior to testing, the coincidence of the axes of the tested DEBs, the load cell, and the loading beam was guaranteed using a laser level. To trace the developed vertical deflection, four linear variable displacement transducers (LVDTs) having a measuring length of 100 mm were positioned at different locations along the span of the tested

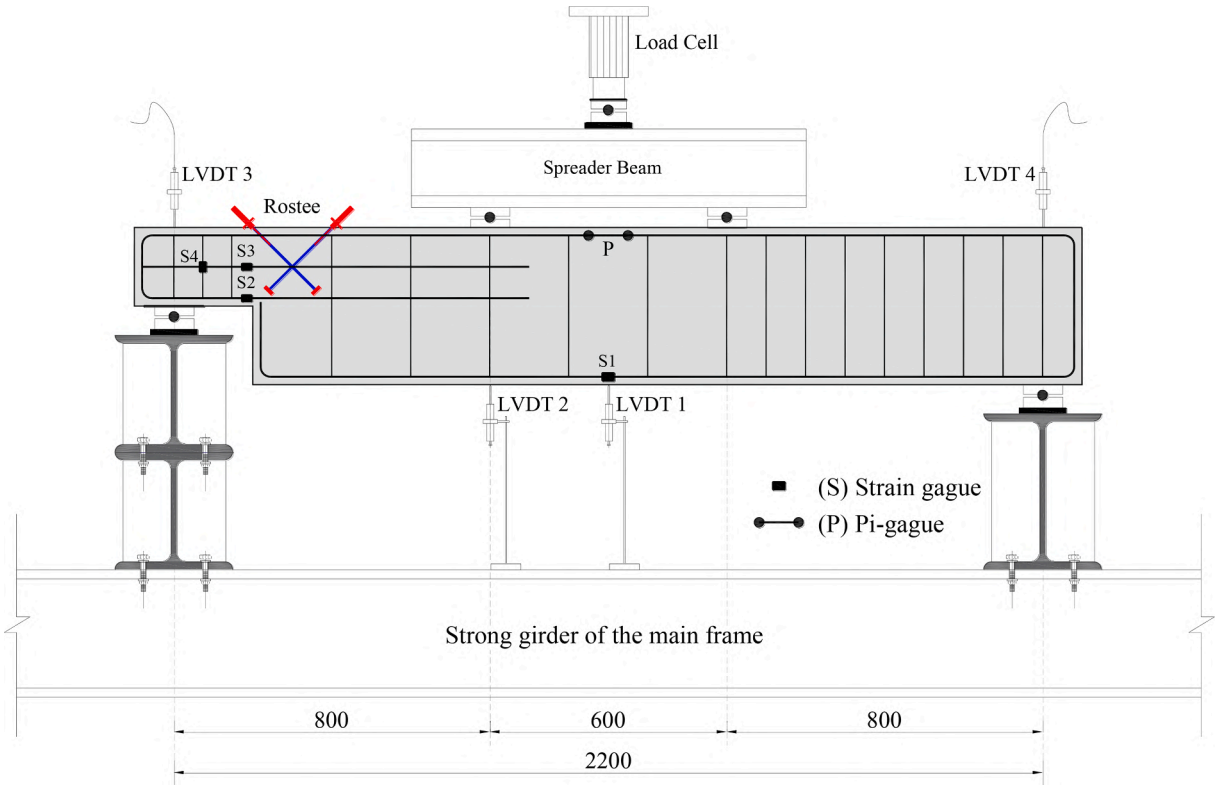



**Fig. 8.** Test setup and instrumentation (All dimensions in mm).

specimens. Two of them were located underneath the loading point near the re-entrant corner and at the mid-span section. Whereas, the rest were situated atop of the supporting points in order to attain the net-deflection of the tested DEBs. Another two-perpendicular rosette LVDTs (45-degree) were placed on the concrete surface at the center of the expected crack line in order to estimate the developed shear strains. To certify the occurrence of shear failure at the re-entrant corner and nowhere else, the developed normal strains on selected internal bars were measured by means of four electrical strain gauges with 10-mm gauge length (S1 to S4), as depicted in Fig. 8. Furthermore, the developed tensile normal strains on the hanger reinforcements (specimen BC-H), diagonal reinforcements (specimen BC-H), and reinforcements embedded inside P-SHCC plates (strengthened DEBs) were measured by 6-mm strain gauges mounted at the point where the maximum stress is expected to occur. Additionally, 100 mm-long Pi-gauges were used to measure the developed compressive strains on the concrete surface at the mid-span section.

The major shear crack width was measured at different load levels using an optical microscope of 0.01 mm accuracy with the aim of verifying the adequacy of the adopted strengthening system in enhancing the serviceability requirements for the tested DEBs. All specimens were loaded in several steps up to failure, where the applied load was measured by a load cell of 500 kN capacity and the average loading rate was about 10 kN/min. After each loading step, an automatic data acquisition unit was used to collect and store data during testing from the load cell, LVDTs, Pi-gauge, and strain gauges.

## 3. Experimental results

### 3.1. Mode of failure

Images of the crack patterns of all tested dapped-end beams (DEBs), either un-strengthened (reference) or strengthened ones, just before the complete failure are shown in Fig. 9(a) through 9(j). With regard to the mode of failure, as expected, all tested DEBs failed in diagonal tension failure stemming from the re-entrant corner without yielding of the tensile flexural bars. Undoubtedly, that is owing to the concentration of shear stresses in this region, besides the fact that these corners were sharp and not gently beveled [74].

In all tested specimens, the first crack appeared at the re-entrant corner at a load ranging between 41 and 53 kN, as listed in Column 3 of Table 5. The lowest cracking load (41 kN) was recorded for the defected reference specimen (BC) at a load level of 52 % of the ultimate load as a result of being devoid of shear reinforcements at the re-entrant corner. Whereas all strengthened DEBs showed higher cracking loads as compared to the control specimen (BC), corresponding to on average 36 % of their ultimate loads due to the superior tensile characteristics of the SHCC materials. Shortly after the shear cracks initiated from the re-entrant corner, flexural cracks at the bottom soffit of the pure moment region were visually detected at a load of about 57 kN for all tested DEBs. With further loading, both shear and flexural cracks gradually widened and extended in length, but this extension was faster in the shear cracks than in the flexural ones at comparable load levels. In the meantime, narrower shear cracking in the full-depth section was observed in some of the tested DEBs. Finally, cracks were uniformly distributed around the re-entrant corner until failure occurred.

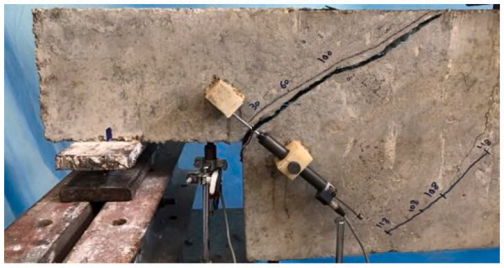
The failure of defected reference specimen (BC) was sudden and brittle, whereas the failure of the two properly detailed reference specimens BC-H and BC-D was governed by yielding of hanger reinforcements ($\varepsilon_s = 1438\ \mu\varepsilon > \varepsilon_y = 1400\ \mu\varepsilon$) and of diagonal reinforcements ($\varepsilon_s = 1541\ \mu\varepsilon > \varepsilon_y = 1400\ \mu\varepsilon$), respectively. On the other hand, the mode of failure of all strengthened specimens was governed by SHCC rupture as well as yielding of the embedded reinforcements (refer to Column 4 of Table 4 and Column 14 of Table 5), with no sign of debonding or delamination between the substrate concrete and the P-SHCC plates as shown in Fig. 9. Besides, the developed shear crack at the re-entrant for DEBs strengthened by P-SHCC plates was narrower, especially in the case of 45°-inclined P-SHCC plates (see discussion below). It was apparently due to the bridging action of the discrete polypropylene discrete fibers comprised inside the P-SHCC plates



a. Specimen BC.



b. Specimen BC-H.



c. Specimen BC-D.



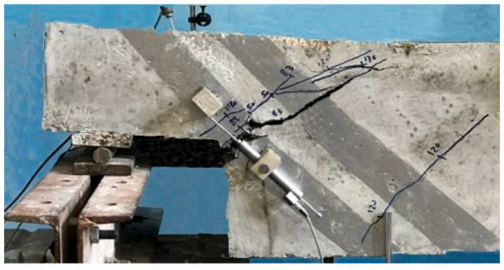
d. Specimen BUE-H1-40.



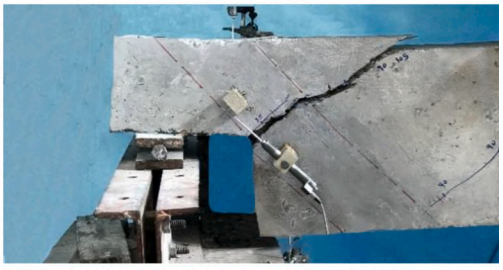
e. Specimen BUE-H2-40.



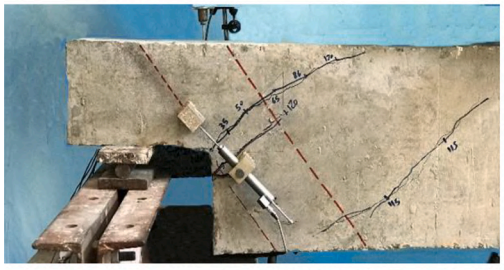
f. Specimen BUE-D1-40.



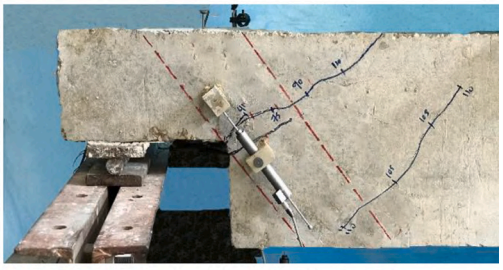
g. Specimen BUE-D2-40.



h. Specimen BUI-D1-40.



i. Specimen BUI-D1-55.



j. Specimen BUI-D1-70.

**Fig. 9.** Failure modes of all tested DEBs.

components.

Until complete failure, the longitudinal flexural reinforcements of all tested DEBs did not reach the yielding strain ($\varepsilon_y$ = 2069 με); refer to Column 15 of Table 5. It could be attributed to the fact that the provided main tensile steel was designed in accordance with PCI guidelines [17] to trigger shear failure at the re-entrant corner of such DEBs prior to any un-wanted mode of failure. As seen in Column 16 of Table 5, the concrete in compression zone did not crush ($\varepsilon_c < \varepsilon_{cu}$ = 3000 με). It was noticeably that, the tensile strains in longitudinal flexural reinforcements and the compression strains for all strengthened DEBs showed higher values than their counterpart reference specimens. This indicates the positive impact of the P-SHCC strengthening system in postponing the brittle shear failure of the strengthened specimens.

**Table 5**
Experimental results.

| (1) | (2) | (3) | (4) | (5) | (6) | (7) | (8) | (9) | (10) | (11) | (12) | (13) | (14) | (15) | (16) |
|---|---|---|---|---|---|---|---|---|---|---|---|---|---|---|---|
| Group No. | Specimen | Loads (kN) | | | Gain in $P_u$ (%) | | | Displacement (mm) | | | | Initial stiffness kN/mm | Strains ($\mu\varepsilon$) | | |
| | | $P_{cr}$ | $P_s$ | $P_u$ | W.R.T BC | W.R.T BC-H | W.R.T BC-D | $\Delta_{cr}$ | $\Delta_s$ | $\Delta_u$ | $\frac{\Delta_u}{\Delta_{u,BC}}$ | | $\varepsilon_{se}$ | $\varepsilon_s$ | $\varepsilon_c$ |
| G1 | BC | 41.0 | 60.1 | 79.6 | — | — | — | 1.69 | 2.53 | 4.30 | 1.00 | 24.26 | — | 952 | 1204 |
| | BC-H | 43.0 | 88.8 | 118.7 | 49.1 | — | — | 1.47 | 3.29 | 5.70 | 1.33 | 29.25 | 1438* | 1154 | 1480 |
| | BC-D | 45.0 | 101.8 | 127.9 | 60.7 | 7.8 | — | 1.43 | 3.67 | 6.20 | 1.44 | 31.47 | 1541** | 1376 | 1784 |
| G2 | BUE-H1-40 | 50.0 | 97.8 | 126.2 | 58.5 | 6.3 | — | 1.45 | 3.57 | 5.94 | 1.38 | 34.48 | 1520 | 1361 | 1763 |
| | BUE-H2-40 | 48.0 | 95.2 | 122.3 | 53.6 | 3.0 | — | 1.48 | 3.41 | 5.85 | 1.36 | 32.43 | 1482 | 1287 | 1663 |
| G3 | BUE-D1-40 | 53.0 | 108.7 | 143.2 | 79.9 | 20.6 | 12.0 | 1.35 | 3.86 | 7.11 | 1.65 | 39.26 | 1754 | 1549 | 2021 |
| | BUE-D2-40 | 51.0 | 104.4 | 135.3 | 69.9 | 14.0 | 5.8 | 1.38 | 3.81 | 6.64 | 1.54 | 36.96 | 1621 | 1427 | 1915 |
| G4 | BUI-D1-40 | 46.0 | 102.9 | 132.1 | 66.0 | 11.3 | 3.3 | 1.31 | 3.74 | 6.54 | 1.52 | 35.11 | 1604 | 1396 | 1811 |
| | BUI-D1-55 | 47.0 | 117.7 | 144.5 | 81.5 | 21.7 | 13.0 | 1.27 | 4.25 | 7.20 | 1.67 | 37.90 | 1799 | 1539 | 2007 |
| | BUI-D1-70 | 48.0 | 123.9 | 152.1 | 91.0 | 28.1 | 18.9 | 1.19 | 4.93 | 7.80 | 1.81 | 40.34 | 1878 | 1632 | 2235 |

$P_{cr}$ = first shear cracking load; $P_s$ = service load; $P_u$ = ultimate load; W.R.T = with respect to; $\Delta_{cr}$ = net mid-span deflection corresponding to the shear cracking load; $\Delta_s$ = net mid-span deflection corresponding to the service load; $\Delta_u$ = net mid-span deflection corresponding to the ultimate load; $\Delta_{u,BC}$ = the ultimate mid-span of the reference specimen BC; $\varepsilon_{se}$ = the maximum tensile strain in the reinforcements embedded inside P-SHCC plates; $\varepsilon_s$ = the maximum tensile strain in the longitudinal flexural reinforcements; $\varepsilon_c$ = the maximum compressive strain in concrete at mid-span section.
* the maximum tensile strain in hanger reinforcements at the re-entrant corner for specimen BC-H.
** the maximum tensile strain in diagonal reinforcements at the re-entrant corner for specimen BC-D.

### 3.2. Ultimate loads

The ultimate load capacity ($P_u$) as well as the gain in $P_u$ for all DEBs as compared to the reference specimens are summarized in Columns 5 to 8 of Table 5. It can be concluded that all strengthened DEBs exhibited higher capacities than their counterparts' un-strengthened DEBs. The overall average gain in $P_u$ for strengthened DEBs was about 71.5 % relative to the defected reference specimen (BC). This average gain demonstrates the successful employment of P-SHCC plates for improving the shear strength of RC dapped-end beams. Moreover, as anticipated, a slightly higher gain in $P_u$ for all strengthened specimens was observed compared with their two properly detailed reference counterparts (BC-H and BC-D); refer to Columns 7 and 8 of Table 5. Of course, as the latter specimens were quantified in order to provide the same tensile force as those of all strengthened specimens. Nevertheless, strengthening of DEBs using P-SHCC plates exhibited more ductile behavior and narrower cracks at the re-entrant corner compared to those correctly designed based on PCI requirements [17], as will be discussed in the next sections.

With regard to the P-SHCC plate scheme, DEBs strengthened with the external continuous P-SHCC plate (BUE-H1-40 and BUE-D1-40) showed a higher increase in terms of the ultimate load capacity than their intermittent/discontinuous counterparts (BUE-H2-40 and BUE-D2-40). This observation emphasizes the pronounced connotation of applying the P-SHCC plate strengthening system as close as possible to the re-entrant corner of DEBs, which is in conformity with the outcomes of Wang et al. [10]. For instance, specimen BUE-D1-40 (strengthened by 45°-inclined continuous P-SHCC plate) failed at an ultimate load of 143.2 kN, which yields a 79.9 % gain in shear capacity with regard to the reference specimen, BC. Substituting the continuous scheme with an intermittent one (BUE-D2-40) decreased the gain in $P_u$ to 69.9 %.

As for P-SHCC plate orientation, DEBs strengthened by 45°-inclined external P-SHCC plates, either with continuous (BUE-D1-40) or intermittent (BUE-D2-40) scheme showed higher ultimate load capacities than their counterparts strengthened by vertical external P-SHCC plates (BUE-H1-40 and BUE-H2-40). This increase was due to the crack-arresting action generated by the 45°-inclined P-SHCC plates, which were placed approximately perpendicular to the expected crack line, resulting in obstructing the developed cracks as compared to that exhibited by their vertical counterparts. Referring to the reference specimen BC, the gain in $P_u$ was higher for specimens BUE-D1-40 (79.9 %) and BUE-D2-40 (69.9 %) than that for specimens BUE-H1-40 (58.5 %) and BUE-H2-40 (53.6 %), respectively.

Regarding the position of the P-SHCC plates, it can be seen that specimens strengthened with internal P-SHCC plates (group No. 4) resulted in a lower enhancement in $P_u$ as compared to their counterparts with external P-SHCC plates (group No. 3). This observation may be apparently due to the fact that the dominant shear crack was tied by the strengthening plate at the central section only in group No. 4 (internally strengthened DEBs), whereas it was arrested on two outer sides in group No. 3 (external P-SHCC plates); refer to Fig. 6. For clarification, the gain in $P_u$ was 79.9 % and 66.0 % for specimens BUE-D1-40 and BUI-D1-40, respectively.

As far as the thickness of the P-SHCC plate is concerned, the ultimate shear capacity for all internally strengthened DEBs was enhanced by increasing the thickness of the P-SHCC plate. Logically, the increase in P-SHCC plate thickness led to an advancement in the contribution of SHCC materials to the shear strength of RC dapped-end beams. Specimen BUI-D1-70, with a 70 mm P-SHCC plate thickness, achieved a higher gain in $P_u$ (91.0 %); refer to Column 6 of Table 5. Specimens BUI-D1-40 and BUI-D1-55 failed at an ultimate load of 132.1 kN and 144.5 kN, which yielded a gain in $P_u$ of about 66.0 % and 81.5 %, respectively. It is worth mentioning that the gain in $P_u$ was not proportional to the thickness of P-SHCC plate. It may be attributed to the fact when the thickness of P-SHCC plates goes up, the thickness of the concrete in the shear-resistant section goes down, but the width of DEBs stays the same.

### 3.3. load–deflection response

The typical load–deflection plots of all tested DEBs are depicted in Fig. 10(a) through 10(d). In addition, the net mid-span deflection corresponding to the cracking, service, and ultimate loads ($\Delta_{cr}$, $\Delta_s$ and $\Delta_u$) is given in Columns 9 to 11 of Table 5, where the service load was taken as the ultimate load divided by the load factor, which equals 1.50 according to Martínez and Meli [18]. Furthermore, the ratio ($\Delta_u/\Delta_{u,BC}$) between the ultimate deflection for any specimen and the ultimate deflection for the defected reference specimen (BC) is listed in the 12th Column of Table 5. It can be observed that $\Delta_u$ was generally higher for all strengthened DEBs when compared to that of the reference specimen

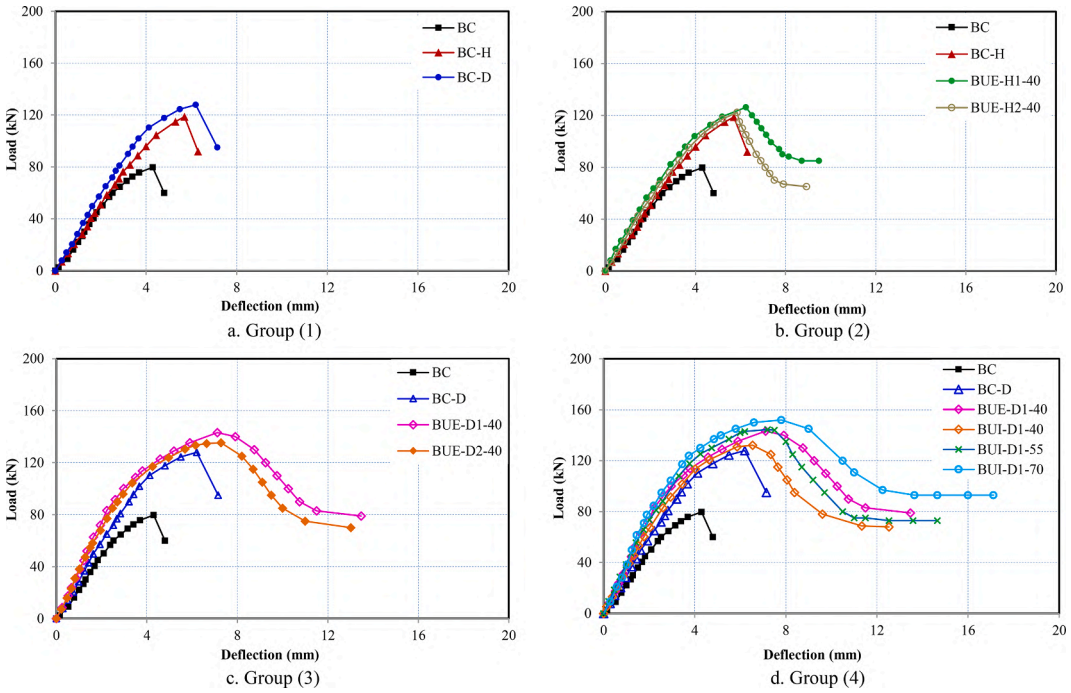



**Fig. 10.** Load-deflection relationships for the tested DEBs.

(BC), with an average value of 1.56 for the ratio $\Delta_u/\Delta_{u,BC}$. For all tested DEBs, different kinds of post-peak behavior have been observed, as shown in Fig. 10. It can be observed that the load–deflection curves for all un-strengthened reference specimens (group No.1) were approximately linear up to near the ultimate load and then dropped suddenly. In contrast, all other strengthened DEBs experienced softening behaviors during the post-peak stage, demonstrating the efficiency of the adopted strengthening system in improving the load–deflection response as well as the ductility of these specimens.

Dapped-end beam's stiffness was calculated as the slope of the load–deflection curve [75] and then recorded in the 13th Column of Table 5. It was noticed that all strengthened DEBs had higher stiffness relative to their counterpart reference specimens, and these values were affected by the studied parameters. Specimens of the external continuous P-SHCC plate scheme (BUE-H1-40 and BUE-D1-40) exhibited higher stiffness than their intermittent P-SHCC plate scheme counterparts (BUE-H2-40 and BUE-D2-40) due to the closeness of the strengthening system to the re-entrant corner of DEBs. Moreover, all DEBs strengthened by 45°-inclined external P-SHCC plates with continuous or intermittent schemes showed higher stiffness than their vertical counterparts. That was a result of the almost perpendicularity between the inclined strengthening system and the potential crack. For

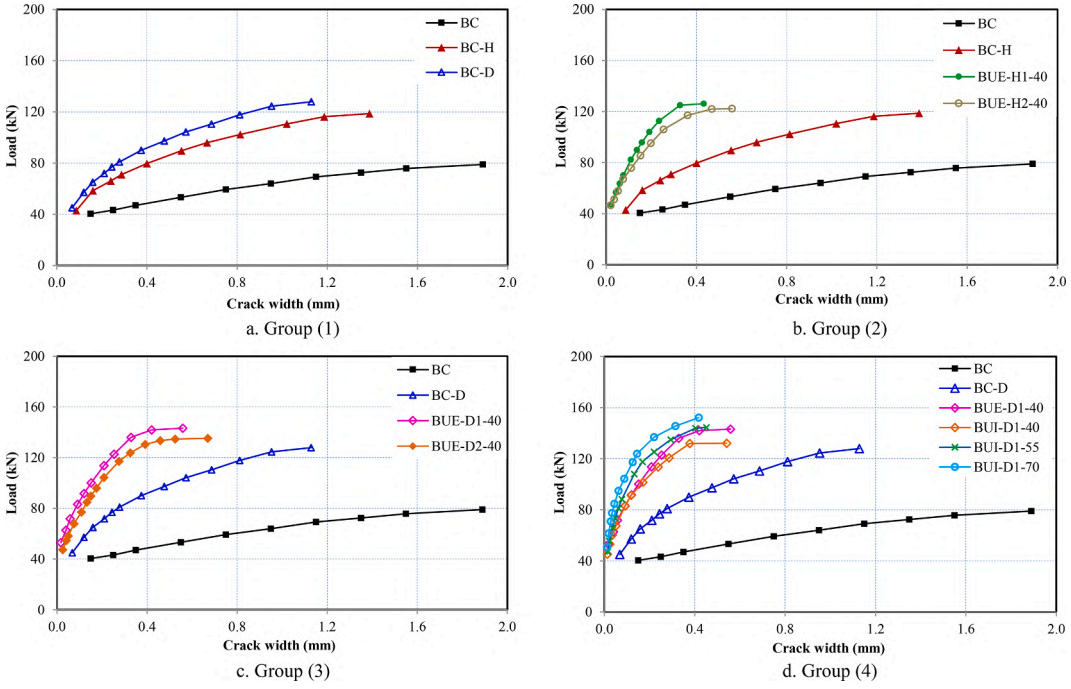



**Fig. 11.** Load-crack width relationships for the tested DEBs.

instance, the initial stiffness was higher for specimen BUE-D1-40 (39.26 kN/mm) than that for specimen BUE-H1-40 (34.48 kN/mm), which was in turn higher than that for specimen BUE-H2-40 (32.43 kN/mm). Changing the position of P-SHCC plates from external to internal lowered the initial stiffness by about 11.0 % for the same P-SHCC plate thickness (40 mm). However, the initial stiffness values were improved by increasing the thickness of the internal P-SHCC plate. For instance, the initial stiffness was higher for specimen BUI-D1-70 (40.34 kN/mm) than that for specimen BUI-D1-55 (37.90 kN/mm), which was in turn higher than that for specimen BUI-D1-40 (35.11 kN/mm).

### 3.4. Crack width analysis

For all tested DEBs, the maximum width of the major shear crack emanating from the re-entrant corner was measured and traced against the applied load as shown in Fig. 11(a) through 11(d). In addition, Table 6 lists these values at different loading levels (45, 76, and 122 kN) as well as at the service and ultimate loads. For the reader's information, the different loading levels were chosen as follows: 45 kN is the load value immediately after cracking of the specimen BC-D (properly detailed reference specimen provided with diagonal reinforcements), 76 kN is the load value just before the failure of the defected reference specimen (BC), and 122 kN is the minimum ultimate load achieved for the strengthened specimens. It can be observed that, at all loading levels, all strengthened DEBs have a considerable reduction in the shear crack width compared to those of the reference specimens.

At about 45 kN, all un-strengthened reference specimens (group No. 1) were cracked, and the associated measured shear crack width for specimens BC, BC-H, and BC-D were 0.302 mm, 0.104 mm, and 0.088 mm; respectively. Nevertheless, all strengthened DEBs did not record any cracking at the same load. Further loading; at about 76 kN, all strengthened DEBs exhibited lower crack widths with an average reduction value of 95.0 % relative to the defected reference specimen (BC). Furthermore, strengthened DEBs with P-SHCC plates exhibited smaller crack width at the re-entrant corner compared to those correctly designed based on PCI requirements [17], with an average value greater than 70 %. This may be attributed to the crack-arresting action of the used P-SHCC plates, which altered the crack propagation compared to that exhibited by reference specimens. Consequently, this observation indicates the effective implementation of the used P-SHCC plates in improving the serviceability behavior of the strengthened specimens.

Regarding the P-SHCC plate scheme, the continuous strengthening systems led to decreased values of the crack width of strengthened DEBs with an average value of 28 % at a load of about 122 kN when compared to the corresponding values of the intermittent counterparts. This observation demonstrates the significant effect of the continuity of P-SHCC plates on the cracking behavior of the strengthened DEBs. As for the orientation of the P-SHCC plate, the crack widths were reduced when using inclined P-SHCC plates as compared to those when using vertical P-SHCC plates. This may be attributed to the fact that when the P-SHCC plates' inclination angle was near the direction of the principal stresses, their efficiency in restricting the developed cracks improved. For instance, specimen BUE-D1-40 showed a crack width of 0.246 mm, while specimen BUE-H1-40 displayed a crack width of 0.314 mm at the same load (122 kN).

In terms of the position of the P-SHCC plates, it is clear that using an internal P-SHCC plate centered on the specimen cross-section resulted in lower enhancement in terms of cracking behavior when compared to external P-SHCC plates attached at the surface of the substrate concrete if they were of the same thickness. At the same load (122 kN), the crack width for specimen BUE-D1-40 (0.246 mm) was smaller than that for specimen BUI-D1-40 (0.321 mm) by about 23 %. As far as the thickness of the P-SHCC plate is concerned, a reduction in the crack width for all internally-strengthened DEBs was obtained by increasing the thickness of P-SHCC plate owing to the extra-contribution of SHCC materials and their outstanding characteristics. At a load level of 122 kN, the DEBs internally strengthened by 55 mm (BUI-D1-55) and 70 mm (BUI-D1-70) P-SHCC plates had smaller crack widths than the BUI-D1-40 specimen by about 33 % and 54 %, respectively.

It is worth mentioning that the same trend of the measured shear cracking width was obtained at both service and ultimate loads for all studied parameters; refer to Columns 6 and 10 of Table 6. This means that the use of P-SHCC plates controlled the crack widths until the ultimate load for the tested DEBs was reached. To emphasize this result, the crack width for all tested DEBs at different loads were plotted, then compared at the service load level with the maximum crack width ($w_{max}$), specified as per *ACI* 318–19 code [65] as shown in Fig. 12. It was obvious that all strengthened DEBs are conservative, unlike un-strengthened reference specimens that either defected or were correctly designed, confirming PCI guidelines [17].

### 3.5. Ductility measurement

Ductility is the ability of the structure to undergo significant inelastic deformation while still resisting loads. So, it is in fact one of the important aspects related to the design of RC structures. In case of reinforced concrete DEBs, not only strength but also ductility plays a significant role in their performance. For the present research, two ductility indicators were selectively chosen, namely, displacement-based ductility ($\mu_\Delta$) and energy-based ductility ($\mu_E$). As per Afefy et al.

**Table 6**
Major diagonal shear crack width at different load levels (mm).

| (1) | (2) | (3) | (4) | (5) | (6) | (7) | (8) | (9) | (10) |
|---|---|---|---|---|---|---|---|---|---|
| Group No. | Specimen | At 45kN | At 76kN | At 122kN | At service load | | | | At ultimate load |
| | | | | | Width | W.R.T BC | W.R.T BC-H | W.R.T BC-D | |
| G1 | BC | 0.302 | 1.562 | — | 0.591 | 1.00 | — | — | 1.89 |
| | BC-H | 0.104 | 0.358 | — | 0.409 | 0.69 | 1.00 | — | 1.39 |
| | BC-D | 0.088 | 0.248 | 0.934 | 0.353 | 0.60 | 0.86 | 1.00 | 1.13 |
| G2 | BUE-H1-40 | — | 0.096 | 0.314 | 0.141 | 0.24 | 0.34 | 0.40 | 0.47 |
| | BUE-H2-40 | — | 0.118 | 0.468 | 0.145 | 0.25 | 0.35 | 0.41 | 0.56 |
| G3 | BUE-D1-40 | — | 0.072 | 0.246 | 0.129 | 0.22 | 0.32 | 0.37 | 0.56 |
| | BUE-D2-40 | — | 0.076 | 0.320 | 0.133 | 0.23 | 0.33 | 0.38 | 0.67 |
| G4 | BUI-D1-40 | — | 0.078 | 0.321 | 0.136 | 0.23 | 0.33 | 0.39 | 0.54 |
| | BUI-D1-55 | — | 0.052 | 0.216 | 0.132 | 0.22 | 0.32 | 0.37 | 0.45 |
| | BUI-D1-70 | — | 0.042 | 0.148 | 0.126 | 0.21 | 0.31 | 0.36 | 0.42 |

W.R.T = with respect to.

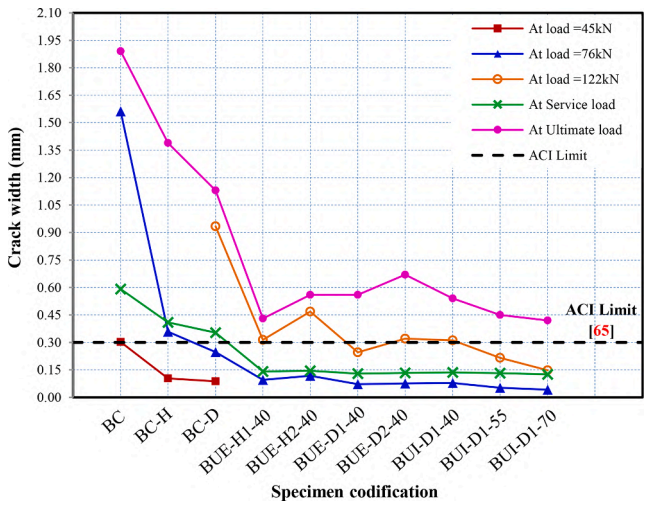



**Fig. 12.** Experimental crack width for all tested DEBs at different load levels.

[76], the displacement ductility index, $\mu_\Delta$, is defined by Eq. (2):

$$\mu_\Delta = \left(\frac{\Delta_{max}}{\Delta_s}\right) \tag{2}$$

where ($\Delta_{max}$) is the mid-span deflection at failure and ($\Delta_s$) is the mid-span deflection corresponding to the service load. The energy ductility index ($\mu_E$) as presented in Eq. (3) is defined as the ratio between the energy of the DEB corresponding to failure ($E_{max}$) and the energy of the DEB related to service load ($E_s$); considering that, the energy (E) can be estimated as the area under the load–deflection plot [76].

$$\mu_E = \left(\frac{E_{max}}{E_s}\right) \tag{3}$$

Table 7 shows the ductility indices for tested DEBs using the aforementioned indicators. It is obvious that both indices approximately experienced the same trend as compared to the relevant ductility of the reference specimens. As can be seen in Columns 6 and 12 of Table 7, relative to the defected reference specimen (BC), the ductility values have been significantly improved due to the proposed strengthening system (P-SHCC plates), with an average increase of more than 65 % considering both the displacement-based and energy-based indices. The greatest increase was observed for specimen BUE-D1-40, which was strengthened by 45°-inclined external continuous P-SHCC plates (84 % with regard to displacement-based index and 110 % considering energy-based index).

Moreover, all strengthened DEBs showed more ductile behavior than their counterparts correctly designed in accordance with PCI requirements [17]. The displacement-based ductility and energy-based indices for strengthened DEBs with vertical P-SHCC plates were greater than specimen BC-H (properly detailed reference specimen provided with hanger reinforcements) by an average value of about 38 % and 21 %, respectively. While DEBs strengthened by 45°-inclined P-SHCC plates exhibited an increase in ductility of more than 75 % considering both displacement-based and energy-based indicators, as compared to specimen BC-D (properly detailed reference specimen provided with diagonal reinforcements). This may be due to the favorable characteristics of the used P-SHCC plates in arresting shear cracks at the re-entrant corner region by fiber bridging action. Consequently, based on these results, it was evident that the proposed strengthening system led to a considerable enhancement in the ductility behavior of the tested DEBs.

## 4. Theoretical analysis

This section introduces two different analytical models for estimating the ultimate shear capacities ($V_{pro}$) as well as the average diagonal crack width ($w_{avg}$) for the strengthened dapped-end beams (DEBs). Moreover, the verification of these proposed models against the experimental results is presented.

### 4.1. A simple model for estimating the ultimate shear capacities

#### 4.1.1. Derivation of shear capacity formula

Based on the mechanical model adopted in Fig. 13, the ultimate shear capacity ($V_{pro}$) of all tested DEBs can be determined by summing the shear capacities of concrete ($V_c$), hanger/diagonal reinforcements ($V_s$), and precast SHCC plates ($V_{SHCC}$), as given in Eq. (4).

$$V_{pro} = V_c + V_s + V_{SHCC} \tag{4}$$

The shear capacity of concrete ($V_c$) was calculated per *ACI* 318–19 [65] by summing the shear carried by the aggregate interlock ($V_{ci}$), the concrete in the compression zone ($V_{cc}$), and the dowel action of longitudinal reinforcement ($V_{cd}$), as given by Eq. (5).

$$V_c = \left[0.16\lambda\sqrt{f'_c} + 17\rho_w\left(\frac{V_u.d}{M_u}\right)\right] b.d \tag{5}$$

**Table 7**
Ductility indices for the tested DEBs.

| (1) | (2) | (3) | (4) | (5) | (6) | (7) | (8) | (9) | (10) | (11) | (12) | (13) | (14) |
|---|---|---|---|---|---|---|---|---|---|---|---|---|---|
| | | Displacement-based ductility | | | | | | Energy-based ductility | | | | | |
| Group No. | Specimen | $\Delta_s$(mm) | $\Delta_{max}$(mm) | $\mu_\Delta = \left(\frac{\Delta_{max}}{\Delta_s}\right)$ | W.R.T BC | W.R.T BC-H | W.R.T BC-D | $E_s$(kN.mm) | $E_{max}$(kN.mm) | $\mu_E = \left(\frac{E_{max}}{E_s}\right)$ | W.R.T BC | W.R.T BC-H | W.R.T BC-D |
| G1 | BC | 2.53 | 4.80 | 1.90 | 1.00 | — | — | 164 | 233 | 1.42 | 1.00 | — | — |
| | BC-H | 3.29 | 6.30 | 1.91 | 1.01 | 1.00 | — | 170 | 261 | 1.54 | 1.08 | 1.00 | — |
| | BC-D | 3.67 | 7.15 | 1.95 | 1.03 | 1.02 | 1.00 | 186 | 312 | 1.68 | 1.18 | 1.09 | 1.00 |
| G2 | BUE-H1-40 | 3.57 | 9.48 | 2.66 | 1.40 | 1.39 | 1.36 | 316 | 614 | 1.94 | 1.37 | 1.26 | 1.15 |
| | BUE-H2-40 | 3.41 | 8.93 | 2.62 | 1.38 | 1.37 | 1.34 | 307 | 549 | 1.79 | 1.26 | 1.16 | 1.07 |
| G3 | BUE-D1-40 | 3.86 | 13.47 | 3.49 | 1.84 | 1.83 | 1.79 | 367 | 1093 | 2.98 | 2.10 | 1.94 | 1.77 |
| | BUE-D2-40 | 3.81 | 13.02 | 3.42 | 1.80 | 1.79 | 1.75 | 338 | 949 | 2.81 | 1.98 | 1.82 | 1.67 |
| G4 | BUI-D1-40 | 3.74 | 12.53 | 3.35 | 1.76 | 1.75 | 1.72 | 299 | 693 | 2.32 | 1.63 | 1.51 | 1.38 |
| | BUI-D1-55 | 4.25 | 14.65 | 3.45 | 1.81 | 1.80 | 1.77 | 313 | 746 | 2.38 | 1.68 | 1.55 | 1.42 |
| | BUI-D1-70 | 4.93 | 17.11 | 3.47 | 1.83 | 1.82 | 1.78 | 323 | 779 | 2.41 | 1.70 | 1.57 | 1.44 |

$\Delta_s$ = mid-span deflection corresponding to the service load; $\Delta_{max}$ = mid-span deflection corresponding to the failure load; $\mu_\Delta$ = displacement-based ductility; W.R.T = with respect to; $E_s$ = energy of the system at the service load; $E_{max}$ = energy of the system at the failure load; $\mu_E$ = energy-based ductility.

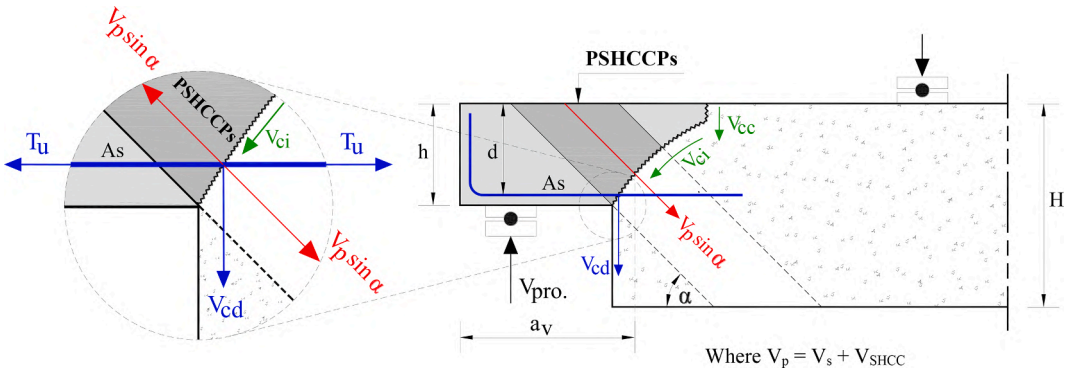



**Fig. 13.** Mechanical model for strengthened DEBs.

where $\lambda$ is a concrete parameter equal to 1.00 for the normal weight concrete, $f_c'$ is the cylinder compressive strength of concrete (refer to Table 3), b is the net width of the concrete section, d is the effective depth of the nib, $\rho_w$ is the longitudinal reinforcement ratio, $V_u$ is the factored shear force at the considered section, and $M_u$ is the corresponding factored moment at that section. For simplicity, the value of $M_u/V_u$ can be replaced by the shear span ($a_v$); see Eq. (6).

$$V_c = \left[0.16\lambda\sqrt{f_c'} + 17\rho_w\left(\frac{d}{a_v}\right)\right]b.d \tag{6}$$

The shear capacity of the hanger/diagonal reinforcements ($V_s$) can be calculated by Eq. (7).

$$V_S = A_S \times f_y \times sin\alpha \tag{7}$$

where $A_S$ is the total area of hanger or diagonal reinforcements even embedded inside the P-SHCC plate, $f_y$ is the tensile yield strength of the used reinforcement (refer to Table 4), and α is the inclination angle of the used reinforcement with horizontal.

The shear capacity of the precast SHCC plates ($V_{SHCC}$) can be estimated by Eq. (8).

$$V_{SHCC} = A_{SHCC} \times f_{ti} \times sin\alpha \tag{8}$$

where $A_{SHCC}$ is the total cross-sectional area of P-SHCC plates and $f_{ti}$ is the tensile strength of SHCC matrix (refer to Table 3).

#### 4.1.2. Verification of the proposed shear capacity formula against the experimental results

To verify the accuracy of the proposed equation for the ultimate shear capacity ($V_{pro}$), the experimental shear capacities for the strengthened DEBs were compared with those obtained from the proposed equation considering all studied parameters, as demonstrated in Table 8. It can be observed that the proposed equation gives conservative shear capacities considering almost all test parameters. In addition, the variation in results of the proposed equation ranged from 3 % to 12 % and the coefficient of variation (COV) was about 8 %. That means that the proposed equation showed satisfactory agreement with the experiment results, with an average error of about 1 %. For more details, an example for the predicted shear capacity of the strengthened specimen BUE-D2-40 is presented in Appendix (A).

### 4.2. A simple model for estimating the average diagonal crack width ($w_{avg}$)

Table 9 presents a review of the previous models to estimate the average diagonal crack width of RC beams [77–80]. It should be noted that all variables mentioned in this paper are explained in the notation. Also, Table 10 shows the experimental results for the average shear crack widths of the strengthened DEBs, which were measured at the service load level, compared to those calculated based on the adopted previous models [77–80]. Obviously, as listed in Table 10, the adopted previous models exhibit un-conservative results and did not consider the effect of using P-SHCC plates in strengthening DEBs, where $w_{avg}(Pred)$ is the estimated diagonal crack width by previous models and $w_{avg}(Exp)$ is the experimental data of the diagonal crack width at the re-entrant corner. Therefore, a new model should be established to take such effects into account.

#### 4.2.1. Derivation of average shear crack width formula

The proposed equation to calculate the average diagonal shear crack width at the re-entrant corner of strengthened DEBs was developed based on strain compatibility and the assumption that there is an almost linear relationship between the average shear crack width ($w_{avg}$), concrete strain ($\varepsilon_{ctr}$) and the developed tensile strain of P-SHCC plate ($\varepsilon_P$); see Eq. (9). Where $l_w$ is the horizontal projection length of the diagonal

**Table 8**
Analytical shear capacities versus experimental results for the strengthened DEBs.

| Specimen | Experimental capacities (kN) | | Proposed capacities (kN) | | | | $V_{exp}/V_{pro}$ |
|---|---|---|---|---|---|---|---|
| | $P_u$ | $V_{exp}$ | $V_c$ | $V_s$ | $V_{SHCC}$ | $V_{pro}$ | |
| BUE-H1-40 | 126.20 | 63.10 | 18.69 | 14.07 | 33.28 | 66.04 | 0.96 |
| BUE-H2-40 | 122.30 | 61.15 | 18.69 | 14.07 | 33.28 | 66.04 | 0.93 |
| BUE-D1-40 | 143.20 | 71.60 | 18.69 | 9.98 | 35.29 | 63.96 | 1.12 |
| BUE-D2-40 | 135.30 | 67.65 | 18.69 | 9.98 | 35.29 | 63.96 | 1.06 |
| BUI-D1-40 | 132.10 | 66.05 | 18.69 | 9.98 | 35.29 | 63.96 | 1.03 |
| BUI-D1-55 | 144.50 | 72.25 | 16.43 | 9.98 | 48.53 | 74.94 | 0.96 |
| BUI-D1-70 | 152.10 | 76.05 | 14.17 | 9.98 | 61.76 | 85.91 | 0.89 |
| Average | | | | | | | 0.99 |
| Standard deviation | | | | | | | 0.08 |
| Coefficient of variation (COV) | | | | | | | 0.08 |

$P_u$ = Experimental ultimate load; $V_{exp}$= experimental ultimate shear capacity = 0.5 $P_u$; $V_c$= concrete resistance; $V_s$= steel resistance; $V_{SHCC}$= SHCC resistance; $V_{pro}$= proposed ultimate shear capacity.

**Table 9**
Overview of previous models predicting the average shear crack width ($w_{avg}$).

| Models | Formulas |
|---|---|
| **Hassan et al.** [77] | $w_{avg} = \frac{d_{by} k_1 k_2 S_l}{1000 k_{f_c} k_w}$<br>$S_l = 4\times10^3\varepsilon_w + 20 \times 10^6(\varepsilon_w)^2$for smooth bars and = $8\times10^3\varepsilon_w + 2 \times 10^6(\varepsilon_w)^2$for deformed bars.<br>$k_w = \left(\frac{\rho_w}{0.004}\right)^{1.3}$ $k_{f_c} = \left(\frac{f_c'}{19.6}\right)^{2/3}$ |
| **Shinomiya &Watanabe** [78] | $w_{avg} = l_{av}\varepsilon_w$<br>$l_{av} = 2\left(\frac{c_s + c_a}{2} + \frac{s}{10}\right) + 0.1\frac{d_{by}}{\rho_y}$<br>$c_a = (s_y - d_{by})/2$ $s = (b_w - 2c_s - d_{by})$ $\rho_y = A_w/[(2c_a + d_{by})b_w]$ |
| **Piyamahant** [79] | $w_{avg} = \frac{2 d_{by} S_l}{(f_c/20)^{2/3}}$<br>$S_l = \varepsilon_w(6 + 3500\varepsilon_w)$ |
| **De silva et al.** [80] | $w_{avg} = k_w S_{m\theta}\varepsilon_w$<br>$k_w = \left(\frac{0.004}{\rho_w}\right)^{2/3}$ $S_{m\theta} = \frac{1}{\frac{\sin\theta}{s_{mx}} + \frac{\cos\theta}{s_{my}}}$<br>$S_{mx} = 2\alpha_1\left(C_x + \frac{S_x}{10}\right) + k_1 k_2 \frac{d_{bx}}{\rho_x}$ $S_{my} = 2\beta_1\left(C_y + \frac{S_y}{10}\right) + k_1 k_2 \frac{d_{by}}{\rho_y}$ |

crack ($l_w = d/\tan\theta$) and $\theta$ denotes the cracking angle of the diagonal crack; assumed to be 30° for the strengthened DEBs, whose properties stay within the scope of the study.

$$w_{avg} = \left[\int_0^{l_w} (\varepsilon_P - \varepsilon_{ctr})dx\right] cos\theta \tag{9}$$

By neglecting the effect of tension stiffening, as the tensile strain of concrete is much smaller than that of SHCC, the average shear crack width can be simplified as shown in Eq. (10). Therefore, the average diagonal crack width can be obtained by integrating Eq. (10), to be as presented in Eq. (11).

$$w_{avg} = \left[\int_0^{l_w} (\varepsilon_P)dx\right] cos\theta \tag{10}$$

$$w_{avg} = \varepsilon_P l_w cos\theta \tag{11}$$

Since there is no sign of debonding or delamination that was experimentally observed, the tensile strain of P-SHCC plate ($\varepsilon_P$), the tensile strain of the used reinforcement ($\varepsilon_S = f_S/E_S$), and the tensile strain in SHCC matrix ($\varepsilon_{SHCC} = f_{ti}/E_{SHCC}$) were almost equal (i.e., $\varepsilon_P = \varepsilon_S = \varepsilon_{SHCC}$). Where $f_S$ is the tensile stress of steel, $E_S$ is the modulus of elasticity of steel and equals 2x10$^5$ MPa, and $E_{SHCC}$ is the modulus of elasticity of SHCC matrix as given in Eq. (12) according to JSCE [72] ($\gamma$ = 23 and $f_{ck}$ is the compressive cylinder strength for SHCC matrix). Then, the model for the average tensile strain of P-SHCC plate ($\varepsilon_P$), can be established, as shown in Eq. (13); where $V$ is the ultimate shear capacity of the DEB.

$$E_{SHCC} = 1.77 \times 10^4 \sqrt{\frac{\gamma}{18.50}} \times \left[\frac{f_{ck}}{60}\right]^{1/3} \tag{12}$$

$$\varepsilon_P = \frac{V - V_c}{(A_{SHCC}E_{SHCC} + A_S E_S) sin\alpha} \tag{13}$$

Therefore, the average diagonal crack width can be calculated by Eq. (14).

$$w_{avg} = \frac{V - V_c}{(A_{SHCC}E_{SHCC} + A_S E_S) sin\alpha} l_w cos\theta \tag{14}$$

**Table 10**
Comparison between the experimental shear crack widths for the strengthened DEBs against estimated ones.

| Specimen | $w_{exp}$(mm) | Hassan et al. [77] | | Shinomiya & Watanabe [78] | | Piyamahant [79] | | De silva et al. [80] | | Proposed model | | |
|---|---|---|---|---|---|---|---|---|---|---|---|---|
| | | $w_{avg}$(mm) | $w_{exp}/w_{avg}$ | $w_{avg}$(mm) | $w_{exp}/w_{avg}$ | $w_{avg}$(mm) | $w_{exp}/w_{avg}$ | $w_{avg}$(mm) | $w_{exp}/w_{avg}$ | $w_{avg}$(mm) | $w_{exp}/w_{avg}$ |
| BUE-H1-40 | 0.141 | 0.816 | 0.17 | 0.29 | 0.49 | 0.488 | 0.29 | 0.784 | 0.18 | 0.131 | 1.08 |
| BUE-H2-40 | 0.145 | 0.816 | 0.18 | 0.29 | 0.50 | 0.488 | 0.30 | 0.784 | 0.18 | 0.131 | 1.11 |
| BUE-D1-40 | 0.129 | 0.677 | 0.19 | 0.29 | 0.44 | 0.488 | 0.26 | 0.784 | 0.16 | 0.122 | 1.05 |
| BUE-D2-40 | 0.133 | 0.677 | 0.20 | 0.29 | 0.46 | 0.488 | 0.27 | 0.784 | 0.17 | 0.122 | 1.09 |
| BUI-D1-40 | 0.136 | 0.677 | 0.20 | 0.29 | 0.47 | 0.488 | 0.28 | 0.784 | 0.17 | 0.122 | 1.11 |
| BUI-D1-55 | 0.132 | 0.405 | 0.33 | 0.29 | 0.46 | 0.488 | 0.27 | 0.522 | 0.25 | 0.118 | 1.12 |
| BUI-D1-70 | 0.126 | 0.271 | 0.46 | 0.28 | 0.45 | 0.488 | 0.26 | 0.399 | 0.32 | 0.115 | 1.10 |
| Average | | | 0.27 | | 0.44 | | 0.29 | | 0.23 | | 1.09 |
| Standard deviation | | | 0.103 | | 0.058 | | 0.014 | | 0.062 | | 0.024 |
| Coefficient of variation (COV) | | | 0.388 | | 0.134 | | 0.048 | | 0.267 | | 0.022 |

$w_{exp}$ = the experimental data of diagonal crack width; $w_{avg}$ = the estimated diagonal crack width by previous models.

#### 4.2.2. Verification of the proposed crack width formula against the experimental results

To assess the accuracy of the above-proposed model, experimental data for the diagonal crack width at the re-entrant corner of strengthened DEBs and theoretical values predicted by the proposed model were compared in Table 10. The average ratio of experimental data to estimated results is 1.09, and the standard deviation is 0.024. Noticeably, the above formula shows high accuracy for predicting the average diagonal crack width ($w_{avr}$) of the strengthened DEBs. For illustration, Appendix (B) includes an example of the predicted average diagonal crack width ($w_{avr}$) for the strengthened specimen BUE-D2-40.

## 5. Conclusion

An experimental program consisting of ten specimens was cast and tested to evaluate the efficiency of precast SHCC (P-SHCC) plates as a strengthening system on the overall performance of dapped-end beams (DEBs). The scheme of P-SHCC plates (continuous or intermittent), the plates' orientation (vertical or diagonal), their position (external or internal), as well as the thickness of the P-SHCC plate served as the test variables. A simple analytical formulation was proposed for the estimation of the ultimate shear capacities ($V_{pro}$) of strengthened DEBs. Additionally, a procedure was developed to calculate the average diagonal crack width ($w_{avg}$). According to the used concrete dimensions and reinforcement detailing, it is possible to extract the following conclusions:

1. The adopted strengthening system (P-SHCC plates) has substantially improved the ultimate shear capacity of all strengthened dapped-end beams (DEBs). The gain in the ultimate load ($P_u$) ranged from 53.6 % to 91.0 %, relative to the reference specimen BC, depending on the test parameters. Moreover, continuous P-SHCC plates scheme has shown to be more effective than intermittent configuration due to the closeness of the strengthening system to the nib's edge.
2. Using 45°-inclined P-SHCC plates had a better effect than that provided by vertical ones, as the P-SHCC plates were approximately positioned to be perpendicular to the expected crack line. The ultimate capacity of specimen BUE-D1-40 (143.2 kN) was about 14 % higher than that of specimen BUE-H1-40 (126.2.2 kN).
3. Specimens externally provided with P-SHCC plates have generally performed better, in terms of the ultimate load carrying capacity, than those strengthened by internal P-SHCC plates counterparts. Furthermore, the ultimate shear capacity was improved by increasing the thickness of the internal P-SHCC plate owing to the advancement in the contribution of SHCC materials to the shear capacity of RC dapped-end beams.
4. The strengthening system (P-SHCC plates) led to improve the deformational characteristics of all strengthened DEBs. The mid-span deflection at ultimate for the strengthened specimens BUE-D1-40 and BUI-D1-70 reached up to 1.67 and 1.81 times, respectively, that reported for specimen BC. Besides, during the post-peak stage, softening behaviors were obtained in all strengthened specimens, representing the ductility improvement of these specimens.
5. An advantage in shear crack width measurements at the re-entrant corner for the strengthened specimens over the reference specimens was revealed, especially when 45° inclined P-SHCC plate was used. At load level of about 76 kN, all strengthened DEBs showed decreased crack widths with an average reduction value of 95.0 % and 70 % relative to the defected reference specimen (BC) and properly designed specimens (BC-H, BC-D), respectively.
6. Regardless of the tested parameters, the adopted strengthening system (P-SHCC plates) has remarkably enhanced the obtained ductility characteristics. The displacement-based and energy-based indices reached up to 84 % and 110 % compared to the reference specimen BC, respectively.
7. Two simple analytical models were presented, one for calculating the ultimate shear capacities ($V_{pro}$) of the strengthened DEBs and the other for predicting the average diagonal crack width ($w_{avg}$) at the re-entrant corner of the strengthened DEBs. The comparisons between the estimated values and the experimental data indicate that the proposed models experience satisfactory accuracy.

**Funding**

The author(s) received no financial support for the research, authorship, and/or publication of this article.

## Declaration of Competing Interest

The authors declare that they have no known competing financial interests or personal relationships that could have appeared to influence the work reported in this paper.

## Appendix (A)

The shear resistance generated by the concrete section ($\boldsymbol{V_c}$)

$$V_c = \left[0.16\lambda\sqrt{f'_c} + 17\rho_w\left(\frac{d}{a_v}\right)\right] b.d$$

$$= \left[0.16 \times 1.0 \times \sqrt{32.6} + 17 \times \frac{226}{(150-40)\times 165} \times \left(\frac{165}{300}\right)\right] \times (150-40) \times 165 = 18694N = 18.69kN$$

The shear resistance generated by reinforcement ($\boldsymbol{V_s}$)

$$V_S = A_S \times f_y \times sin\alpha = (0.84\% \times 40 \times 150) \times 280 \times sin45 = 9979N = 9.98kN$$

The shear resistance generated by P-SHCC plate ($\boldsymbol{V_{SHCC}}$)

$$V_{SHCC} = A_{SHCC} \times f_{ti} \times sin\alpha = (40 \times 150) \times 8.32 \times sin45 = 35299N = 35.29kN$$

The ultimate shear capacity ($\boldsymbol{V_{pro}}$)

$$V_{pro} = V_c + V_s + V_{SHCC} = 18.69 + 9.98 + 35.29 = 63.96\,kN$$

$$V_{exp} = 67.65kN$$

$$\frac{V_{exp}}{V_{pro}} = \frac{67.65}{63.96} = 1.06$$

## Appendix (B)

The average shear crack width ($w_{avg}$)

$$E_{SHCC} = 1.77 \times 10^4 \sqrt{\frac{\gamma}{18.50}} \times \left[\frac{f_{ck}}{60}\right]^{1/3}$$

$$= 1.77 \times 10^4 \sqrt{\frac{23}{18.50}} \times \left[\frac{61.45}{60}\right]^{1/3} = 19893 \text{ MPa}$$

$$\varepsilon_P = \frac{V - V_c}{(A_{SHCC}E_{SHCC} + A_S E_S)sin\alpha}$$

$$= \frac{(63.96 - 18.69) \times 1000}{(40 \times 150 \times 19893 + (0.84\% \times 40 \times 150) \times 200000\,)sin45} = 495 \times 10^{-6}$$

$$w_{avg} = \varepsilon_P l_w cos\theta$$

$$= 495 \times 10^{-6} \times \frac{165}{tan30} \times cos30 = 0.122mm$$

$$\frac{w_{avg,exp.}}{w_{avg}} = \frac{0.133}{0.122} = 1.09$$

As shown in the previous examples, the proposed predictions tend to be in good agreement with the experimental results.

## References


[1] Botros AW, Klein GJ, Lucier GW, Rizkalla SH, Zia P. Dapped ends of prestressed concrete thin-stemmed members: Part 1, experimental testing and behavior. PCI J https:// 2017. https://doi.org/10.15554/pcij62.2-05.

[2] Nagy-György T, Sas G, Dăescu AC, Barros JA, Stoian V. Experimental and numerical assessment of the effectiveness of FRP-based strengthening configurations for dapped-end RC beams. Eng Struct 2012;44:291–303. https://doi.org/10.1016/j.engstruct.2012.06.006.

[3] Taher SD. Strengthening of critically designed girders with dapped ends. Proc Inst Civ Eng: Struct Build 2005;158(2):141–52. https://doi.org/10.1680/stbu.2005.158.2.141.

[4] Desnerck P, Lees JM, Morley CT. Strut-and-tie models for deteriorated reinforced concrete half-joints. Eng Struct 2018;161:41–54. https://doi.org/10.1016/j.engstruct.2018.01.013.

[5] Mattock AH, Chan TC. Design and behavior of dapped-end beams. PCI J 1979;24(6):28–45. https://doi.org/10.15554/pcij.11011979.28.45.

[6] Lu WY, Lin IJ, Yu HW. Behaviour of reinforced concrete dapped-end beams. Mag Concr Res 2012;64(9):793–805. https://doi.org/10.1680/macr.11.00116.

[7] Herzinger R. Stud reinforcements in dapped-ends of concrete beams. Calgary, Canada: University of Calgary; 2008. Ph.D. thesis.

[8] Desnerck P, Lees JM, Morley CT. Impact of the reinforcement layout on the load capacity of reinforced concrete half-joints. Eng Struct 2016;127:227–39. https://doi.org/10.1016/j.engstruct.2016.08.061.

[9] Mata-Falcón J, Pallarés L, Miguel PF. Proposal and experimental validation of simplified strut-and-tie models on dapped-end beams. Eng Struct 2019;183:594–609. https://doi.org/10.1016/j.engstruct.2019.01.010.

[10] Wang Q, Guo Z, Hoogenboom PC. Experimental investigation on the shear capacity of RC dapped end beams and design recommendations. Struct Eng Mech 2005;21(2):221. https://doi.org/10.12989/sem.2005.21.2.221.

[11] Aswin M, Mohammed BS, Liew MS, Syed ZI. Shear failure of RC dapped-end beams. Adv Mater Sci Eng 2015;2015. https://doi.org/10.1155/2015/309135.

[12] Atta A, Taman M. Innovative method for strengthening dapped-end beams using an external prestressing technique. Mater Struct 2016;49(8):3005–19. https://doi.org/10.1617/s11527-015-0701-8.

[13] Ramirez JA, French CW, Adebar PE, Bonacci JF, Collins MP, Darwin D. Recent approaches to shear design of structural concrete. J Struct Eng 1998;124(12):1374. https://doi.org/10.1061/(asce)0733-9445(1998)124:12(1375).

[14] Sas, G., Dăescu, C., Popescu, C. and Nagy-György, T., 2014. Numerical optimization of strengthening disturbed regions of dapped-end beams using NSM and EBR CFRP. Compos. B. Eng., 67, pp.381-390.https://doi.org/10.1016/j.compositesb.2014.07.013.

[15] Chen, B.S., Hagenberger, M.J. and Breen, J.E., 2002. Evaluation of strut-and-tie modeling applied to dapped beam with opening. ACI Struct. J., 99(4), pp.445-450. https://doi.org/10.14359/12113.

[16] Yindeesuk S. Design and analysis of complex D-Regions in reinforced concrete structures. University of Illinois at 2009. Urbana-Champaign.

[17] Institute PC, PCI design handbook, 8th Edition - (MNL-120-17),. Chicago. Illinois https:// 2017. https://doi.org/10.15554/mnl-120-17.

[18] Moreno-Martínez JY, Meli R. Experimental study on the structural behavior of concrete dapped-end beams. Eng Struct 2014;75:152–63. https://doi.org/10.1016/j.engstruct.2014.05.051.

[19] Gemi, L., Aksoylu, C., Yazman, Ş., Özkılıç, Y.O. and Arslan, M.H., 2019. Experimental investigation of shear capacity and damage analysis of thinned end prefabricated concrete purlins strengthened by CFRP composite. Compos. Struct., 229, p.111399.https://doi.org/10.1016/j.compstruct.2019.111399.

[20] Johnson P, Couture A, Nicolet R, 2007. Commission of inquiry into the collapse of a portion of the de la Concorde overpass - report.

[21] Mata-Falcon J. Serviceability and ultimate behaviour of dapped-end beams (In Spanish: Estudio del comportamiento en servicio y rotura de los apoyos a media madera). Spain: Universitat Politecnica de Valencia; 2015. p. 719. PhD thesis.

[22] Reynolds GC. The strength of half-joints in reinforced concrete beams. Cement and Concrete Association 1969.

[23] Mattock AH, Theryo TS. Strength of precast prestressed concrete members with dapped ends. PCI J 1986;31(5):58–75. https://doi.org/10.15554/pcij.09011986.58.75.

[24] Clark LA, Thorogood P. Serviceability behaviour of reinforced concrete half joints. Struct Eng 1988;66(18).

[25] Nanni A, Huang PC. Validation of an alternative reinforcing detail for the dapped ends of prestressed double tees. PCI J 2002;47:38–49. https://doi.org/10.15554/pcij.01012002.38.49.

[26] Lin, I.J., Hwang, S.J., Lu, W.Y. and Tsai, J.T., 2003. Shear strength of reinforced concrete dapped-end beams. Struct. Eng. Mech.: An international journal, 16(3), pp.275-294. https://doi.org/10.12989/sem.2003.16. 3.275.

[27] Desnerck P, Lees JM, Morley CT. The effect of local reinforcing bar reductions and anchorage zone cracking on the load capacity of RC half-joints. Eng Struct 2017;152:865–77. https://doi.org/10.1016/j.engstruct.2017.09.021.

[28] Özkılıç YO, Aksoylu C, Arslan MH. Experimental and numerical investigations of steel fiber reinforced concrete dapped-end purlins. J Build Eng 2021;36:102119. https://doi.org/10.1016/j.jobe.2020.102119.

[29] Zamri NF, Mohamed RN, Elliott KS. Shear capacity of precast half-joint beams with steel fibre reinforced self-compacting concrete. Constr Build Mater 2021;272:121813. https://doi.org/10.1016/j.conbuildmat.2020.121813.

[30] Rajapakse C, Degée H, Mihaylov B. Investigation of shear and flexural failures of dapped-end connections with orthogonal reinforcement. Eng Struct 2022;260:114233. https://doi.org/10.1016/j.engstruct.2022.114233.

[31] Mihaylov B, Rajapakse C, Berger PH. Effect of steel fibers on the ultimate flexural behavior of dapped-end connections. Eng Struct 2022;259:114147. https://doi.org/10.1016/j.engstruct.2022.114147.

[32] Aksoylu C, Özkılıç YO, Arslan MH. Damages on prefabricated concrete dapped-end purlins due to snow loads and a novel reinforcement detail. Eng Struct 2020;225:111225. https://doi.org/10.1016/j.engstruct.2020.111225.

[33] Tan, K.H., 2001. Shear strengthening of dapped beams using FRP systems. In FRPRCS-5: Fibre-reinforced plastics for reinforced concrete structures Volume 1: Proceedings of the fifth international conference on fibre-reinforced plastics for reinforced concrete structures, Cambridge, UK, 16–18 July 2001 (pp. 249-258). Thomas Telford Publishing. https://doi.org/10.1201/9781439832448.ch5.

[34] Özkılıç, Y.O., Yazman, Ş., Aksoylu, C., Arslan, M.H. and Gemi, L., 2021. Numerical investigation of the parameters influencing the behavior of dapped end prefabricated concrete purlins with and without CFRP strengthening. Constr. Build. Mater., 275, p.122173.https://doi.org/10.1016/j.conbuildmat.2020.122173.

[35] Mufti AA. FRPs and FOSs lead to innovation in Canadian civil engineering structures. Constr Build Mater 2003;17(6–7):379–87. https://doi.org/10.2749/222137806796184987.

[36] Nanni A. Flexural behavior and design of RC members using FRP reinforcement. J Struct Eng 1993;119(11):3344–59. https://doi.org/10.1061/(asce)0733-9445(1993)119:11(3344).
[37] Ahmed A, Kodur V. The experimental behavior of FRP-strengthened RC beams subjected to design fire exposure. Eng Struct 2011;33(7):2201–11. https://doi.org/10.1016/j.engstruct.2011.03.010.
[38] Li VC, 1992. Performance driven design of fiber reinforced cementitious composites. In: R.N. Swamy (Ed.) 4th RILEM International Symposium on Fiber Reinforced Concrete, 12-30. https://doi.org/10.1201/9781482271225-8.
[39] Li VC, Wu HC, 1992. Pseudo strain-hardening design in cementitious composites, High Performance Fiber Reinforced Composites, RILEM, Edited by H.W. Reinhardt and A. E. Naaman, 371-87. https://doi.org/10.1115/1.3119767.
[40] Li VC. From micromechanics to structural engineering - The design of cementitious composites for civil engineering applications. J Struct Mech Earthquake Eng 1993;10(2):37–48. https://doi.org/10.2208/jscej.1993.471_1.
[41] Li VC, Mishra DK, Naaman AE, Wight JK, LaFave JM, Wu HC, et al. On the shear behavior of engineered cementitious composites. Advfn Cem Bas Mat 1994;1(3):142–9. https://doi.org/10.1016/1065-7355(94)90045-0.
[42] Li, V. and Fischer, G., 2006. International RILEM Workshop on High Performance Fiber Reinforced Cementitious Composites (HPFRCC) in Structural Applications: Proceedings. RILEM.
[43] Li, K.F., Yang, C.Q., Zhao, Y.B., Pan, Y., Wang, G., Zheng, Y.Y. and Xu, F., 2020. Study on the creep behavior of PVA-ECC based on fractional-differential rheological model. Constr. Build. Mater., 230, p.117064.https://doi.org/10.1016/j.conbuildmat.2019.117064.
[44] Li VC., 2008. Engineered Cementitious Composites (ECC) - Material, Structural, and Durability Performance. In Concrete Construction Engineering Handbook, Chap. 24, Ed. E. Nawy. https://doi.org/10.1201/9781420007657-29.
[45] Kobayashi K, Le Ahn D, Rokugo K. Effects of crack properties and water-cement ratio on the chloride proofing performance of cracked SHCC suffering from chloride attack. Cem Concr Compos 2016;69:18–27. https://doi.org/10.1016/j.cemconcomp.2016.03.002.
[46] Li, V.C., 2019. Engineered cementitious composites (ECC): bendable concrete for sustainable and resilient infrastructure. Springer Berlin Heidelberg. New York, 335-8. https://doi.org/10.1007/978-3-662-58438-5_9.
[47] Lepech MD, Li VC. Application of ECC for bridge deck link slabs. Mater Struct 2009;42(9):1185–95. https://doi.org/10.1617/s11527-009-9544-5.
[48] Afefy HMED, Mahmoud MH. Structural performance of RC slabs provided by pre-cast ECC strips in tension cover zone. Constr Build Mater 2014;65:103–13. https://doi.org/10.1016/j.conbuildmat.2014.04.096.
[49] El-Shafiey, T. F., Hussein, M., Baraghith, A.T. and Hindawi, M, 2022. Enhancement the behavior of RC concentric columns using SHCC tubes. In 13th International conference on sustainable green construction and nanotechnology, Sharm El-Shaikh, Egypt.
[50] Atta AM, Khalil AEH. Improving the failure mode of over-reinforced concrete beams using strain-hardening cementitious composites. J Perform Constr Facil 2016;30(5):04016003. https://doi.org/10.1061/(asce)cf.1943-5509.0000857.
[51] Baraghith AT, Mansour W, Behiry RN, Fayed S. Effectiveness of SHCC strips reinforced with glass fiber textile mesh layers for shear strengthening of RC beams: Experimental and numerical assessments. Constr Build Mater 2022;327:127036. https://doi.org/10.1016/j.conbuildmat.2022.127036.
[52] Khalil, A.E.H., Etman, E., Atta, A. and Essam, M., 2017. Behavior of RC beams strengthened with strain hardening cementitious composites (SHCC) subjected to monotonic and repeated loads. Eng. Struct., 140, pp.151-163.https://doi.org/10.1016/j.engstruct.2017.02.049.
[53] Afefy HM, Baraghith AT, Hassan A, Abuzaid MK. Strengthening of shear-deficient RC beams using near surface embedded precast cement-based composite plates (PCBCPs). Eng Struct 2021;244:112765. https://doi.org/10.1016/j.engstruct.2021.112765.
[54] Afefy HM, Baraghith AT, Mahmoud MH. Retrofitting of defected reinforced-concrete cantilever slabs using different techniques. Mag Concr Res 2020;72(14):703–19. https://doi.org/10.1680/jmacr.18.00340.
[55] Elnagar AB, Afefy HM, Baraghith AT, Mahmoud MH. Experimental and numerical investigations on the impact resistance of SHCC-strengthened RC Slabs subjected to drop weight loading. Constr Build Mater 2019;229:116866. https://doi.org/10.1016/j.conbuildmat.2019.116866.
[56] Zhang R, Meng Q, Shui Q, He W, Chen K, Liang M, et al. Cyclic response of RC composite bridge columns with precast PP-ECC jackets in the region of plastic hinges. Compos Struct 2019;221:110844. https://doi.org/10.1016/j.compstruct.2019.04.016.
[57] Mahmoud MH, Afefy HM, Baraghith AT, Elnagar AB. Impact and static behavior of strain-hardening cementitious composites–strengthened reinforced concrete slabs. Adv Struct Eng 2020;23(8):1614–28. https://doi.org/10.1177/1369433219898099.
[58] Ding Z, Wen J, Li X, Fu J, Ji X. Mechanical behaviour of polyvinyl alcohol-engineered cementitious composites (PVA-ECC) tunnel linings subjected to vertical load. Tunn Undergr Space Technol 2020;95:103151. https://doi.org/10.1016/j.tust.2019.103151.
[59] Hassan A, Baraghith AT, Atta AM, El-Shafiey TF. Retrofitting of shear-damaged RC T-beams using U-shaped SHCC jacket. Eng Struct 2021;245:112892. https://doi.org/10.1016/j.engstruct.2021.112892.
[60] Li K, Wei Y, Li Y, Li Z, Zhu J. Flexural behavior of reinforced concrete beams strengthened with high-strength stainless steel wire rope meshes reinforced ECC. Constr Build Mater 2023;362:129627. https://doi.org/10.2139/ssrn.4196443.
[61] Zhou C, Xie Y, Wang W, Zheng Y. Performance-based design for improving impact resistance of RC bridge piers with CFRP grid-reinforced ECC. Eng Struct 2023;275:115217. https://doi.org/10.1016/j.engstruct.2022.115217.
[62] Li S, Chan TM, Young B. Experimental investigation on axial compressive behavior of novel FRP-ECC-HSC composite short column. Compos Struct 2023;303:116285. https://doi.org/10.1016/j.compstruct.2022.116285.
[63] Mohammed BS, Aswin M, Liew MS, Zawawi NAWA. Structural performance of RC and R-ECC dapped-end beams based on the role of hanger or diagonal reinforcements combined by ECC. Int J Concr Struct Mater 2019;13(1):1–19. https://doi.org/10.1186/s40069-019-0356-x.
[64] Mohammed BS, Aswin M, Liew MS. Prediction of failure load of RC and R-ECC dapped-end beams. Case Stud Constr Mater 2020;13:e00433.
[65] ACI Committee 318-19, 2019. Building Code Requirements for Structural Concrete (ACI 318-19) and Commentary (ACI 318R-19). American Concrete Institute, Farmington Hills, MI, 519 ppfv.
[66] ASTM C39/C39M-21, 2021. Standard Test Method for Compressive Strength of Cylindrical Concrete Specimens, ASTM International. www.astm.org.
[67] Astm c293, c293m-16,. Standard Test Method for Flexural Strength of Concrete (Using Simple Beam with Center-Point Loading), ASTM. International 2016. www.astm.org.
[68] ASTM C496/C496M-17, 2017. Standard Test Method for Splitting Tensile Strength of Cylindrical Concrete Specimens, ASTM International. www.astm.org.
[69] ASTM C469/C469M-14, 2014. Standard Test Method for Static Modulus of Elasticity and Poisson's ratio of Concrete in Compression, ASTM International. www.astm.org.
[70] ASTM D2936-20, 2020. Standard Test Method for Direct Tensile Strength of Intact Rock Core Specimens, ASTM International.www.astm.org.
[71] ASTM A615/A615M-16, 2016. Standard specification for deformed and plain carbon steel bars for concrete reinforcement, ASTM International. www.astm.org.
[72] Japan Society of Civil Engineers, 2008. Recommendations for design and construction of high-performance fiber reinforced cement composite with multiple fine cracks (HPFRCC). Concrete engineering series 82.
[73] O-BASF. https://www.basf.com/eg.
[74] Cook WD, Mitchell D. Studies of disturbed regions near discontinuities in reinforced concrete members. ACI Struct J 1988;85(2):206–16. https://doi.org/10.14359/2772.
[75] Khalil AEH, Etman E, Atta A, Baraghith A, Behiry R. The effective width in shear design of wide-shallow beams: a comparative study. KSCE J Civ Eng 2019;23(4):1670–81. https://doi.org/10.1007/s12205-019-0830-7.
[76] Afefy HM, Sennah K, Cofini A. Retrofitting actual-size precracked precast prestressed concrete double-Tee girders using externally bonded CFRP sheets. J Perform Constr Facil 2016;30(2):04015020. https://doi.org/10.1061/(asce)cf.1943-5509.0000763.
[77] Hassan HM. Shear cracking behavior and shear resisting mechanism of reinforced concrete beams with web reinforcement. The University of Tokyo; 1988. Doctoral Dissertation,.
[78] Shinomiya K, Watanabe F. Study on prediction of shear crack width for reinforced concrete beams. Architectural Institute of Japan (AIJ) 2002:295–6.
[79] Piyamahant S. Shear behavior of reinforced concrete beams with a small amount of web reinforcement. Kochi University of Technology; 2002.
[80] De Silva S, Mutsuyoshi H, Witchukreangkrai E. Evaluation of shear crack width in I-shaped prestressed reinforced concrete beams. J Adv Concr Technol 2008;6(3):443–58. https://doi.org/10.3151/jact.6.443.